JOURNAL OF THE AMERICAN WATER RESOURCES ASSOCIATION

AMERICAN WATER RESOURCES ASSOCIATION

A Numerical Study of Hypoxia in Chesapeake Bay Using an Unstructured Grid Model: Validation and Sensitivity to Bathymetry Representation

Xun Cai, Yinglong J. Zhang, Jian Shen, Harry Wang, Zhengui Wang, Qubin Qin, and Fei Ye

Research Impact Statement: This study demonstrates the importance of having an accurate representation of bathymetry with high-resolution unstructured grid to correctly simulate water quality processes in the Chesapeake Bay.

ABSTRACT: A three-dimensional unstructured-grid hydrodynamic and water quality model (Semi-implicit Cross-scale Hydroscience Intergrated System Model-Integrated Compartment Model) is applied successfully for Chesapeake Bay. The model is validated with observations of salinity, chlorophyll-a, dissolved oxygen, nutrients, and phytoplankton productions from the year 1991 to 1995 for the mainstem and some major tributaries, based on multiple model skill scores. Model experiments are conducted to test the importance of having (1) an accurate representation of bathymetry to correctly predict hypoxia and other processes and (2) a high-resolution model grid for tributaries to correctly simulate water quality variables. Comparison with the model experiment results with bathymetry smoothing indicates that bathymetry smoothing, as commonly used for many systems, changes the stratification and lateral circulation pattern, resulting in more salt intrusion into shallow water regions, and an increase in the freshwater age. Consequently, a model with bathymetry smoothing can lead to an unrealistic prediction of the distribution of hypoxia and phytoplankton production. Local grid refinement shows significant improvement of model simulations on local stratification and water quality variables. Overall, the use of high-resolution unstructured grid model leads to a faithful representation of the complex geometry, and thus a seamless cross-scale capability for simulating water quality processes in the Bay including tributaries and tidal creeks.

(KEYWORDS: SCHISM; bathymetry; Chesapeake Bay; water quality; modeling; cross-scale; hypoxia.)

INTRODUCTION

As one of the largest and most productive estuaries in the United States, Chesapeake Bay plays a significant role in serving wildlife and human beings. Chesapeake Bay has been continuously affected by human activities, such as urbanization and agricultural overfertilization, which leads to eutrophication and algal blooms (Nixon 1995). Hypoxia, defined as dissolved oxygen (DO) concentration lower than 2 mg/L, is one of the severe consequences related to eutrophication and algal blooms (Seliger et al. 1985). In summer, hypoxia of Chesapeake Bay is generally caused by strengthened vertical stratification, accelerated respiration of organic matter sinking from spring bloom, and reduced solubility in warmer water that decreases oxygen supply from the water surface (Taft et al. 1980; Kemp et al. 1992; Murphy et al. 2011). Stratification largely reduces DO vertical exchange, preventing the transport of surface DO-rich water to the bottom; the remineralization of

Paper No. JAWR-20-0023-P of the *Journal of the American Water Resources Association* (JAWR). Received February 28, 2020; accepted September 20, 2020. © 2020 American Water Resources Association. **Discussions are open until six months from issue publication**.

Virginia Institute of Marine Science (Cai, Zhang, Shen, Wang, Qin, Ye), William & Mary Gloucester Point, Virginia, USA; and School of Marine Science (Wang), University of Maine Orono, Maine, USA (Correspondence to Cai: ncai@vims.edu).

Citation: Cai, X., Y.J. Zhang, J. Shen, H. Wang, Z. Wang, Q. Qin, and F. Ye. 2020. "A Numerical Study of Hypoxia in Chesapeake Bay Using an Unstructured Grid Model: Validation and Sensitivity to Bathymetry Representation." *Journal of the American Water Resources Association* 1–24. https://doi.org/10.1111/1752-1688.12887.

organic matter accumulated in the bottom water and sediment further consumes DO. Furthermore, nutrient fluxes from the bottom sediment induce summer algal bloom that further increases water column respiration. Therefore, seasonal hypoxia has been observed in Chesapeake Bay since the 1930s (Newcombe and Horne 1938).

Numerical modeling has been applied to study the complex ecosystem of Chesapeake Bay since the late last century (Cerco 1995; Cerco and Noel 2013). Working hand in hand with observation, numerical modeling helps to fill the observation gaps and to quantitatively and qualitatively understand the ecological processes and mechanisms (Cerco 1995). Different types of models have been utilized in the past several decades in Chesapeake Bay, from simplified conceptual or statistical models (Murphy et al. 2011; Lee et al. 2013) to complex three-dimensional hydrodynamic-biogeochemical models (Cerco 1995; Park et al. 1995; Cerco 2000; Xu and Hood 2006; Li et al. 2009; Lanerolle et al. 2010; Brown et al. 2013; Testa et al. 2014; Feng et al. 2015; Xia and Jiang 2016). In particular, the fully coupled three-dimensional hydrodynamic-biogeochemical models can describe well the nonlinear interactions of various processes, and are more frequently used in forecasting and policy making (Irby et al. 2016). An inter-model comparison for eight complex models has been conducted by Irby et al. (2016) and they concluded that all these models have similar skills on simulating magnitude and seasonal variability of DO in the mainstem of the Bay. However, the unstructured-grid (UG) models have the flexibility to resolve the complex coastline, and to use locally fine-resolution grids for small tributaries, where Xia and Jiang (2016) showed such an application. Sufficient resolutions as enabled by unstructured models provide cross-scale capability in capturing more realistic physical processes and relevant interactions in shallow areas and tributaries, which, in turn, improves the simulations of water quality variables (Cai et al. this issue; Cerco and Noel 2013; Xia and Jiang 2016). Despite the great promise shown by UG models, significant challenges remained until recently. As explained in Ye et al. (2018), bathymetry representation in models requires further scrutiny as it underpins a model's representation of physical processes such as gravitational circulation and freshwater plume. Another important consideration for water quality simulation is the computational efficiency in the face of high resolution used to resolve small tributaries and creeks, which may exert outsized influence for Bay water quality (Xia and Jiang 2016). Traditional explicit or split explicit models are limited by stability constraints that require small time steps for high resolution.

SCHISM (Semi-implicit Cross-scale Hydroscience Integrated System Model) has been applied to Chesapeake Bay by Ye et al. (2018) with several major improvements from previous models: (1) high-resolution triangular-quadrangular unstructured horizontal grid and novel hybrid vertical grid with shaved cells near the bottom (Zhang et al. 2015), (2) semi-implicit numerical algorithm which allows relatively large time steps (e.g., 150s in this study) with very fine resolution, and (3) an accurate non-smoothed representation of the original bathymetry (Zhang et al. 2016; Ye et al. 2018). With the high model skill obtained on the simulation of hydrodynamics, in this paper we proceed to coupling SCHISM with a water quality model to study the seasonal hypoxia in Chesapeake Bay, with special attention paid to the importance of accurate representation of bathymetry and its impact on water quality simulation. In Methods section, we describe the available data, model setup, and analysis methods used in this study. Results of a 5-year (1991–1995) study selected in this study because they are the primary benchmark management period for U.S. Environmental Protection Agency (USEPA) simulation and model skill assessments are presented in Model Assessment section. In Discussion section, we discuss the effects of non-smoothed bathymetry on model simulations of hypoxia and other related processes. The model's flexibility is demonstrated in a tributary by applying two grids with or without local refinements. A short conclusion is presented in Summary and Conclusion section.

METHODS

Available Monitoring Data and Watershed Loadings

We utilize the database of water quality monitoring network from the Chesapeake Bay Program (CBP), in the main Bay and its tributaries since 1984 (http://www.chesapeakebay.net/data). These biogeochemical data are generally measured once (winter) or twice (summer) a month. The measurements are conducted at the surface, above the pycnocline, below the pycnocline, and near the bottom, respectively. There is wide coverage of variables — including nutrients, sediments, planktons, water temperature, salinity, and DO. In addition to this database, long-term observed data used by Harding et al. (2002) are also used in this study for some cross comparisons to calibrate the modeled phytoplankton production.

The watershed of Chesapeake Bay covers an area of about 167,000 km^2, which includes parts of New York, Pennsylvania, Delaware, Maryland, Virginia, West Virginia, and the District of Columbia (Kemp et al.

2005). The watershed loading information used in this study is from the Phase 6 Watershed Model of the Chesapeake Bay Assessment Tool (Shenk and Linker 2013). The top three major sources of freshwater flow into the Bay are the Susquehanna, Potomac, and James Rivers. In terms of volume flux, the upper Bay (mainly the Susquehanna River) contributes 58.93% on average for 1991–1995 of the total inflow. The upper Bay watershed loading contributes 60.50% on average of dissolved inorganic nitrogen, and 43.19% of total inorganic phosphorus (TIP). Among the years from 1991 to 1995, 1993 and 1994 are two wet years. The maximum spring discharge is over 1.15 km^3/day and the loadings of inorganic phosphorus are over 100,320 kg/year for 1993 and 74,862 kg/year for 1994, respectively, which are more than twice of the other years. The annual loadings of dissolved inorganic nitrogen are 1,633,000 kg/year for 1993 and 1,598,900 kg/year for 1994, respectively, which are about 50% larger than other years (Figure 1).

Model Description: SCHISM-ICM

SCHISM (Zhang et al. 2016; schism.wiki) is a derivative product of the original Semi-implicit Eulerian Lagrangian Finite Element model (Zhang and Baptista 2008). It is an open-source community-supported modeling system based on unstructured grids, designed for seamless simulation of 3D baroclinic circulation across creek-lake-river-estuary-shelf-ocean scales (Zhang et al. 2016). The main features of SCHISM include a semi-implicit time stepping scheme applied in a hybrid finite-element and finite-volume framework to solve the Navier–Stokes equations in hydrostatic form, and as a result, the time step is not restricted by the Courant–Friedrichs–Lewy condition, thus improving numerical efficiency. The Eulerian–Lagrangian method is used to treat the momentum advection to further boost numerical efficiency and stability. The superior stability afforded by SCHISM and its flexible vertical gridding system (Zhang et al. 2015) allows it to use non-smoothed bathymetry to faithfully represent physical processes; the detrimental effects of bathymetry smoothing as commonly used for terrain-following coordinate models have been documented in Ye et al. (2018).

ICM (Integrated Compartment Model), which is originally developed by U.S. Army Corps of Engineering Research and Development Center as one of the components of the water quality model package to

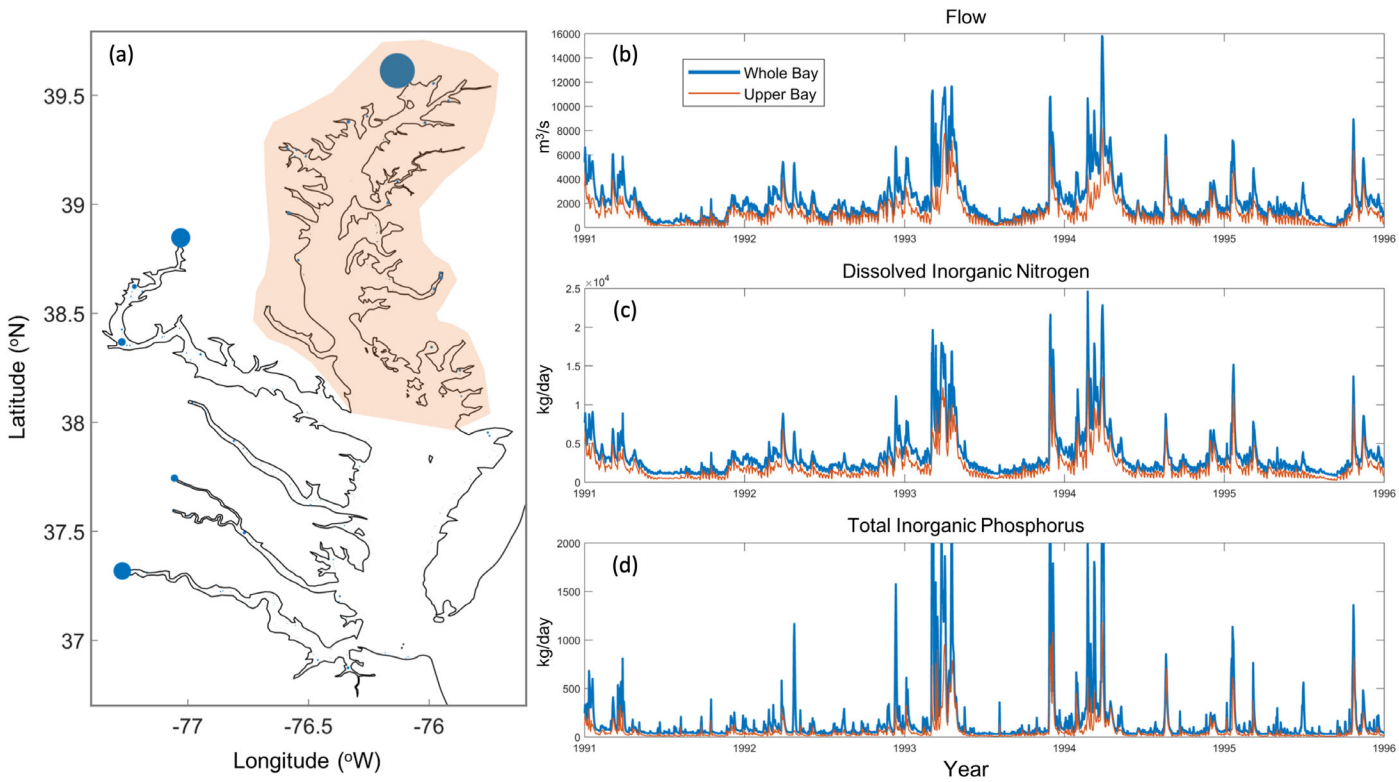

FIGURE 1. (a) Distribution of averaged annual water loading into the Chesapeake Bay in blue spots proportional to the magnitude. (b–d) Time series of total loading of flow, dissolved inorganic nitrogen and total inorganic phosphorus (TIP) from the whole Bay and upper Bay (marked in orange in panel a).

study the eutrophication processes in the Chesapeake Bay, is a flexible, widely applicable eutrophication model (Cerco and Cole 1994). The fully coupled SCHISM-ICM represents a 3D hydrodynamic and eutrophication model, where SCHISM provides physical transport fields and ICM simulates the spatial and temporal distribution of 21 water quality state variables by solving a mass-balance equation for local biological kinetic processes (Park et al. 1995). The local kinetic processes of ICM cover the interactions between phytoplankton, nutrients, and DO in the water column (Figure 2). The photosynthesis of phytoplankton consumes inorganic nutrients and produces DO, while respiration consumes DO and recycles nutrients. Meanwhile, the remineralization of organic nutrients and carbon in the water column further consumes DO. Reaeration provides sources of oxygen from the atmosphere. The sediment flux model developed by Di Toro and Fitzpatrick (1993) was incorporated into ICM, which simulates remineralization processes in the sediment (Figure 2). The sediment flux model is driven by the net settling of particulate organic carbon, nitrogen, phosphorus, and silica from the overlying water column and outputs the sediment oxygen demand and inorganic nutrients fluxes into the water column through remineralization processes.

Model Setup

The model setup closely follows that for a previous hydrodynamic study presented in Ye et al. (2018). In this study, the grid still covers the entire Bay from Cape Henry near the entrance to the Conowingo Dam in the Susquehanna River. The ocean side is still from Lewes, Delaware in the north to Beaufort Inlet, North Carolina in the south, but the offshore boundary is cut along the shelf break to boost computational efficiency (Figure 3). The grid contains 27,374 nodes and 43,009 elements. The resolution varies from about 2.4 km for the continental shelf to 550 m for the main channel near the Bay mouth and 250 m for Upper Bay and tributaries, with a minimum grid size of ~100 m. The new flexible vertical grid system LSC^2 (Localized Sigma Coordinates with Shaved Cells) as developed by Zhang et al. (2015) consists of a variable number of levels from deep (52 layers at 1,000 m depth) to shallow (11 layers at 6 m depth); the average number of vertical in the whole domain is 33.4.

The model was forced at the open boundary by elevation interpolated from two tide gauges at Lewes, Delaware and Beaufort, North Carolina, using inverse distance interpolation method. 15 km around the ocean boundary, salinity, and temperature are nudged to prescribed values as follows, with a maximum relaxation time scale of one day. The ocean salinity is nudged to World Ocean Atlas' monthly climatological data. The temperature is nudged to the Simple Ocean Data Assimilation (SODA) from January 1, 1991 to October 6, 1992 (when HYCOM is not available) and HYCOM from October 7, 1992 to December 31, 1995. As the Gulf Stream cuts through part of the model domain we rely on SODA and HYCOM to bring its signal in and out of the domain. Atmospheric forcing, such as wind and radiation fluxes, is derived from the North American Regional Reanalysis (Mesinger et al. 2006). A non-split time step of 150 s is used in this model. Vertically implicit transport solver TVD^2 (two total variation diminishings; Ye et al. 2016) is applied for the main Bay and ocean part. The horizontal solver uses TVD in the deeper depths (>5 m) and upwind solver for the shallow depths. The vertical turbulence mixing scheme used in this model is k-k1.

The algal assemblage group, diatom (PB1), green algae (PB2), and cyanobacteria (PB3), along with three groups of carbon, five groups of nitrogen, four groups of phosphorus, chemical oxygen demand, and DO, are simulated in the model. Sediment flux model is activated and has been warmed up over 5 years before the simulations. Key parameters are listed in Table 1.

Analysis Methods

Besides directly comparing the outputs of physical and water quality variables, we also calculate the phytoplankton production and freshwater age from the Susquehanna River. We integrate over the water column for each element to get the local phytoplankton production:

$$\mathrm{PP} = \sum_{n=1}^{n} (\mathrm{PB1}_n \cdot \mathrm{GP1}_n + \mathrm{PB2}_n \cdot \mathrm{GP2}_n + \mathrm{PB3}_n \cdot \mathrm{GP3}_n) \cdot \mathrm{dep}_n,$$

where PP is the phytoplankton production (g C/m^2/day). PB1, PB2, and PB3 are three groups (diatom, green algae, and cyanobacteria) of phytoplankton carbon-based concentration in this element over each layer respectively (g C/m^3). GP1, GP2, and GP3 are growth rates of the three phytoplankton groups (day^{-1}), n is layer number and dep is layer thickness (m).

To calculate the age, age tracers are injected from the Susquehanna River. The method is based on the work of Deleersnijder et al. (2001) and Shen and Haas (2004).

Estimation of Hypoxic Volume

Observed profile DO data at stations (as used by Bever et al. 2013) are interpolated/extrapolated into the current SCHISM UG grid to cover the entire Chesapeake Bay. The DO profiles are firstly interpolated

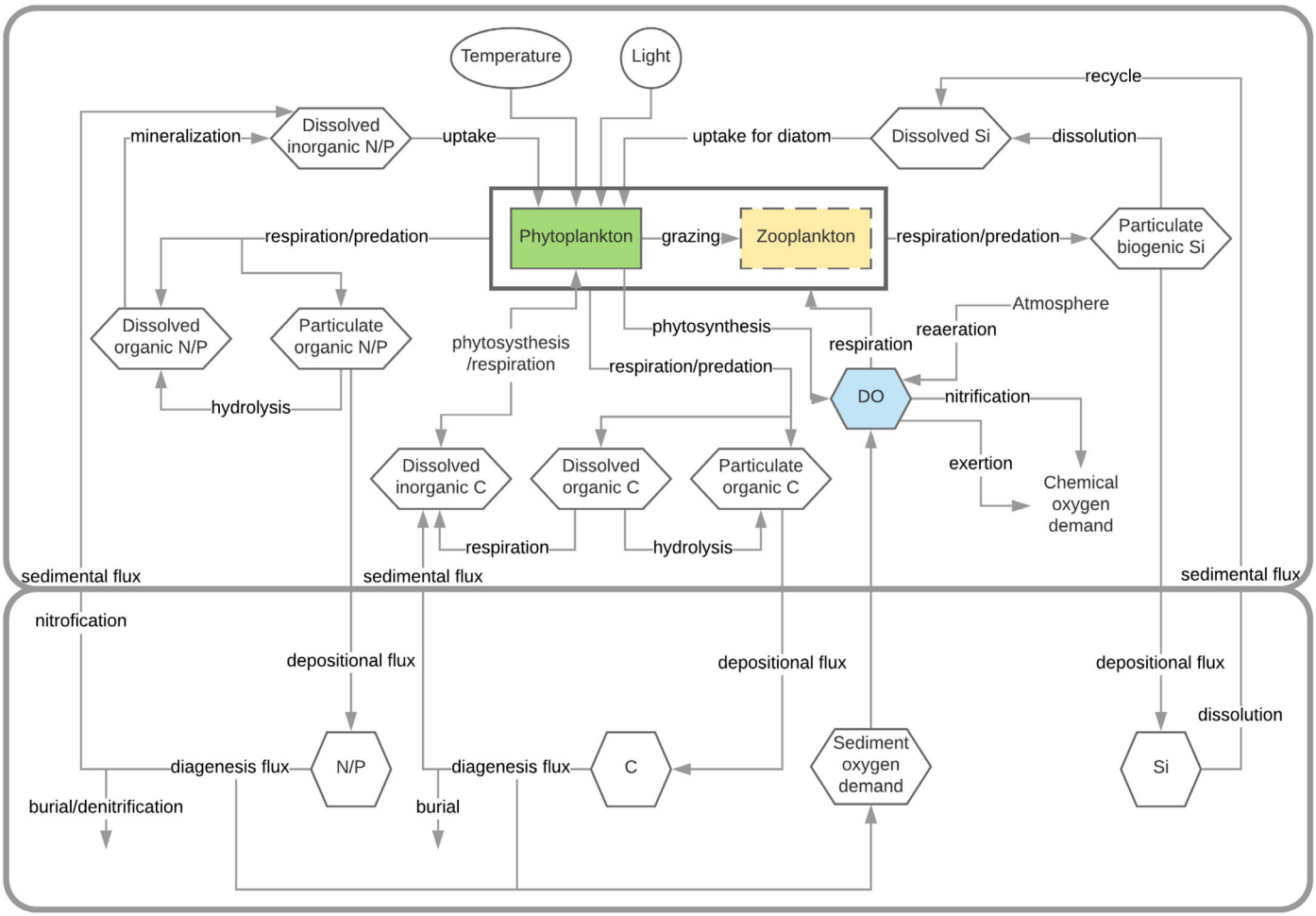

FIGURE 2. Integrated Compartment Model (ICM) eutrophication model schematic (Cerco 2000).

onto 0.1 m vertical resolution with linear interpolation/extrapolation with a minimum value of zero from the surface down to the seabed. And then the interpolated observations of each vertical layer are linearly interpolated horizontally onto every UG grid node. Sensitivity to the UG grid resolution is also tested with convergence achieved within 1% when the resolution is doubted, and therefore the "observed values" reported here are accurate. The hypoxic layer thickness is calculated at each node and the hypoxic volume at each element is the product of the element area and averaged hypoxic layer thickness among the three/four nodes.

MODEL ASSESSMENT

Salinity and Temperature

CBP observations along the transect of the main stem are first used to evaluate model skills (Figure 4). In Figure 4a, 4b, the observations are represented by colored circles so that the model skill is highest if the circles completely disappeared into the background. In addition, observations including other stations from 1991 to 1995 are also used for whole Bay comparisons in the form of a target diagram (Figure 4c). The overall RMSE (root mean square error) are 2.08 practical salinity unit (PSU) for surface salinity and 2.04 PSU for bottom salinity, respectively, which are slightly lower than the skill scores reported in Ye et al. (2018). The corresponding RMSE for temperature are 1.47°C and 2.05°C, respectively, for surface and bottom. Therefore, the model is able to capture temporal and spatial variabilities reasonably for both salinity and temperature (Figure 4). The transect along the main channel in Figure 4b gives information on the averaged salinity profile. The salinity profile is generally well captured by the model throughout the whole Bay, with slight over-estimations at certain lower-Bay stations (e.g., CB7.3). The stratification in the mid-lower Bay is slightly over-estimated. The bottom salinity distribution as shown in Figure 4a suggests that the

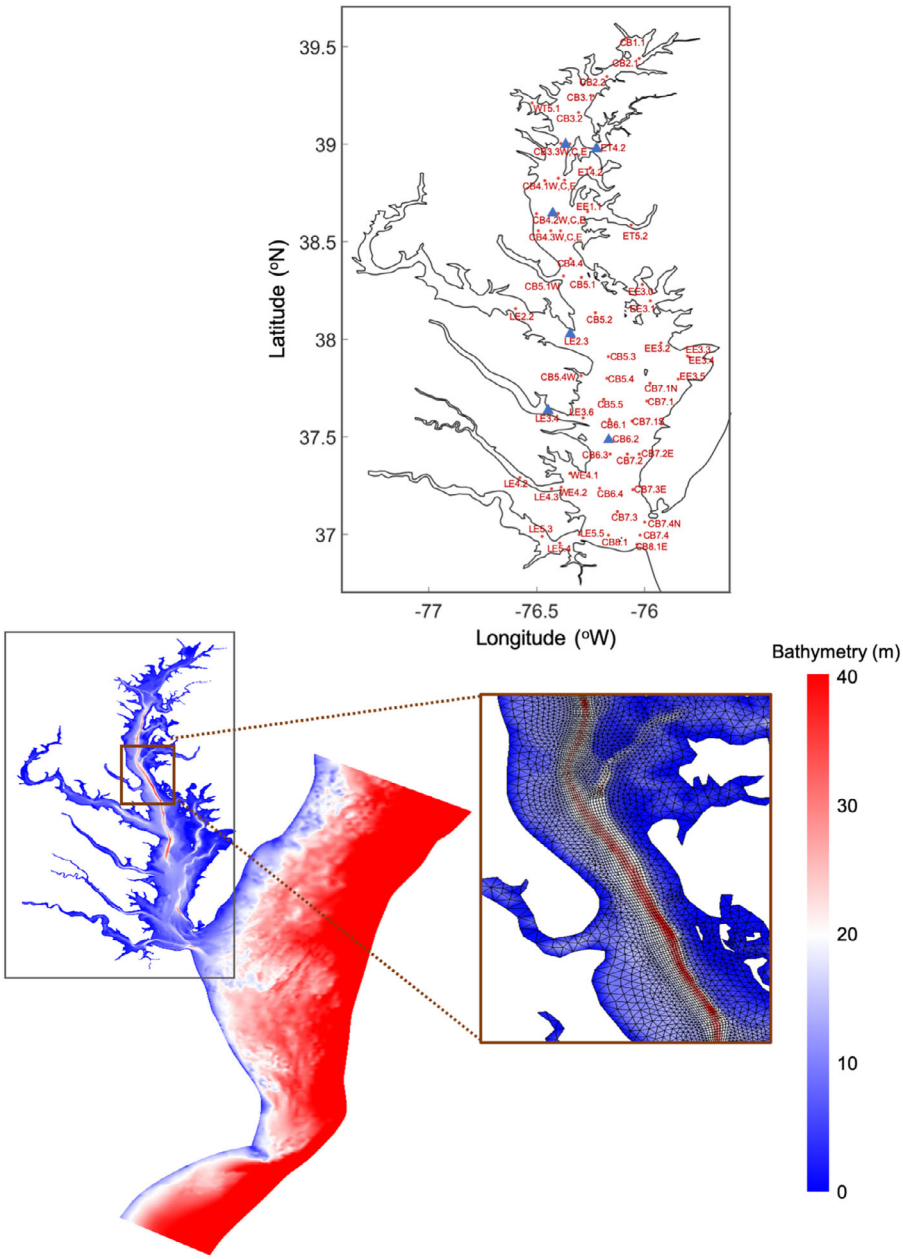

FIGURE 3. Model grid and major Chesapeake Bay Program (CBP) stations used in this paper, where highlighted blue triangles represent the stations shown in Figure 5.

model captures the salt intrusion in the channel and shallow areas equally well. Note that while aggregated skill scores such as those shown in Figure 4 and in Irby et al. (2016) are useful first assessment, they often miss important pieces of information on the temporal and 3D variability as well as key processes such as runaway stratification observed in the mid and upper Bay. More detailed comparisons such as CTD profiles are needed to holistically assess qualitative and quantitative skills of the model. These detailed comparisons are omitted here for brevity but can be viewed in Ye et al. (2018) for a different period (2011–2014). In general, the model is often able to capture the variability of stratifications both in the main stem and in the tributaries (provided that adequate resolution is used there; cf. Estimation of the Effects of Sea-Level Rise with Non-smoothed Bathymetry section). This is mostly attributed to a few model features including higher-order monotonic transport, faithful representation of the underlying bathymetry, and flexibility as provided by the 3D gridding system.

TABLE 1. Key parameters of ICM used in this study.

Parameter	Unit	Value		
		PB1	PB2	PB3
Algae				
Maximum growth rate	day^{-1}	3.5	2.4	1.5
Optimal temperature for growth	°C	10	20	27
Carbon to Chlorophyll a ratio	g C per g Chl	50	60	60
Basel metabolism rate at temperature of 20°C	day^{-1}	0.02	0.02	0.04
Predation rate at temperature of 20°C	day^{-1}	0.3	0.2	0.1
Settling velocity	m/day	0.6	0.4	0.075
Half saturation of nitrogen	g N/m^3	0.01	0.01	0.01
Half saturation of phosphorus	g P/m^3	0.001	0.001	0.001
	Unit	**Carbon**	**Nitrogen**	**Phosphorus**
Nutrients				
Dissolution/hydrolysis rate of RPOM	day^{-1}	0.01	0.005	0.01
Dissolution/hydrolysis rate of LPOM	day^{-1}	0.045	0.075	0.05
Heterotrophic respiration/mineralization rate of DOM	day^{-1}	0.04	0.11	0.05
Settling velocity of POM	m/day	0.4	0.4	0.4
Maximum nitrification rate at temperature of 24°C	g N/m^3/day	—	0.1	—

Notes: DOM, dissolved organic matter; LPOM, labile particulate organic matter; PB1, diatom; PB2, green algae; PB3, cyanobacteria; POM, particulate organic matter; RPOM, refractory particulate organic matter.

Water Quality State Variables and Hypoxia

Model predictions of selected water quality state variables are extensively compared with CBP observations along the main channel and in some tributaries in 1991–1995. RMSE, CC (correlation coefficient), and RE (relative error) are used to assess model errors against observations at both surface and bottom (Table 2). Complementing the table of statistics is the time series comparison at typical stations in upper, mid, lower Bay, and some tributaries as shown in Figures 5 and 6.

The model captures the seasonal cycles and interannual variability of chlorophyll-a, DO, and NO_3^- (Figure 5). Most spring/summer blooms are captured by the model in terms of both timing and magnitude, although there is some over-estimation of bottom chlorophyll-a when concentration is very low at some stations. DO is reasonably predicted by the model with low RMSE (normalized RMSE close to 0.75 for the surface and close to 0.5 for the bottom), high CC (>0.65), and low RE (<20%). The overall RMSE of DO is 1.53 g/m^3 for surface and 1.93 g/m^3 for bottom. The modeled bottom DO correlates well with observations with a slightly delayed recovery in fall (Figure 5). Bottom low DO is captured well at all of the selected typical stations except for over-estimations at CB6.2 and LE3.4. The modeled inorganic nitrogen has high correlations with observations (i.e., CC >0.65 for surface and > 0.5 for bottom). Surface NO_3^- is well captured by the model at all stations. The modeled total organic nitrogen and total phosphorus have relatively low correlations with observations but low RMSE and RE (Table 2), which suggests the modeled values are within a reasonable range of observations. A comparison of the seasonal cycle of phytoplankton production from observations by Harding et al. (2002) suggests that the model shows a sensible cycle and magnitude in different parts of the Bay, with over-estimations for spring and in the upper Bay (Figure 6). However, since the observations are monthly mean values for 17 years (1982–1998), with uncertainty up to 0.7 g C/m^2/day, the model seems reasonable in predicting the phytoplankton productions.

The hypoxic volume we estimated from observations agrees well with the result from CBP volumetric inverse distance squared interpolator program version 4.63 (USEPA 2003; Bever et al. 2013). And the model reasonably captured the observed hypoxic volume (Figure 7). The difference between model estimation and observation interpolation for averaged hypoxic volume from June to August is mostly smaller than 1 km^3 except for the year 1993 when an extraordinarily large hypoxic volume is observed. The predicted along-channel distributions of summer hypoxia are in good agreement with both synoptic summer surveys and 5-year averaged observations (Figure 8). For the synoptic comparison, 20 main stem stations covered by the monitoring cruise are temporally averaged over a 5-day cruise window and then spatially interpolated to generate the along-channel distributions (Figure 8a–8e). These plots

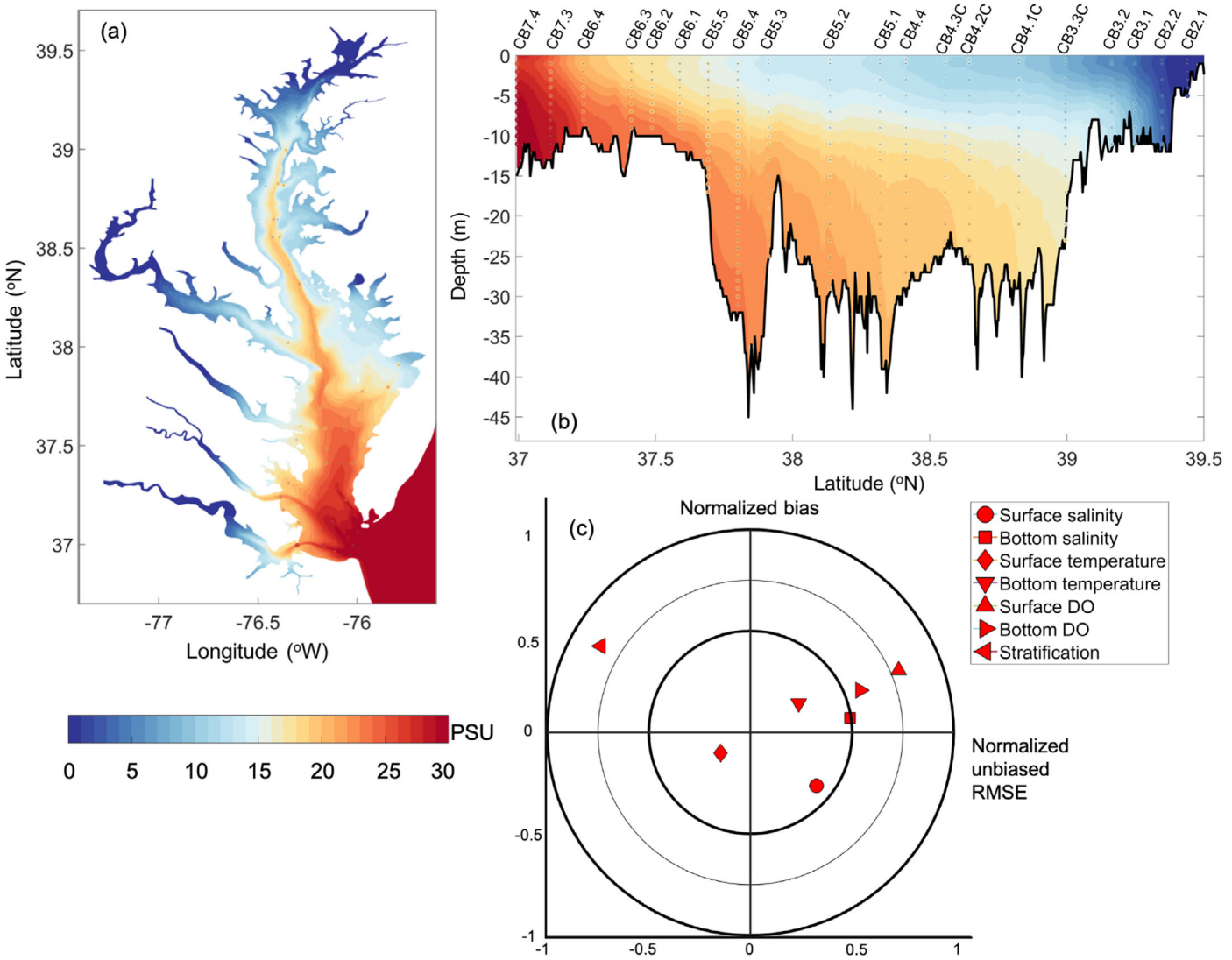

FIGURE 4. Five-year averages of salinity (a) over the Bay bottom and (b) along the main stem. The colored contours represent model results; the colored circles with gray "+" represent CBP observations. (c) Target diagram for salinity, temperature, dissolved oxygen (DO), and stratification model skill at all main stem stations (but stations with fewer than 60 3D measurement points are excluded). RMSE, root mean square error.

demonstrate that the model is capable of capturing the key features of the along-channel distributions of hypoxia, including the location of the oxycline. To assess the model's ability to capture the along-channel severity of the hypoxia during June 1 to September 30 of the 5 years, the bottom DO is compared at all main stem stations (Figure 8f). The model results are averaged over a 5-day window around each survey. Figure 8f demonstrates the good prediction of the hypoxic zone (<2 g/m^3) along the main stem, with slight over-estimations of 0.8–1.5 g/m^3 for the lower Bay (in the non-hypoxic zone). The comparison of the averaged bottom DO with observations suggests a broad agreement in the upper Bay, shoal area, and major tributaries (Figure 8g–8k).

DISCUSSION

Importance of Bathymetry on Simulating Hypoxia in Chesapeake Bay

Model Experiment with Bathymetry Smoothing. One of the reasons for the high model skill of SCHISM on hydrodynamics is attributed to an accurate representation of bathymetry (Ye et al. 2018). Therefore, in this paper, we study the model sensitivity to the bathymetry for water quality variables. A numerical sensitivity experiment, similar to the one shown in Ye et al. (2018), is conducted to expound the importance of bathymetry in predicting hypoxia.

TABLE 2. RMSE, correlation coefficient (CC) and relative error (RE) for model-data comparisons of certain water quality state variables from 1991 to 1995. Model outputs are interpolated onto the corresponding observation times at both surface and bottom to calculate the metrics (NaN due to insufficient amount of observations).

Region	Station	Index	Layer	SAL	CHL	DO	NO_3^-	DIN	TON	TP
Upper bay	CB3.3C	RMSE	S	2.84	23.02	2.11	1.80	0.20	0.23	2.84
			B	2.06	19.12	2.41	2.32	0.13	0.19	2.06
		CC	S	0.89	−0.07	0.66	0.28	0.87	0.85	0.89
			B	0.73	0.12	0.75	−0.05	0.70	0.76	0.73
		RE (%)	S	24.66	7.17	3.83	56.94	7.61	17.85	24.66
			B	6.65	70.15	10.14	83.19	17.87	42.76	6.65
	CB4.1C	RMSE	S	2.40	9.44	1.75	1.98	0.16	0.19	2.40
			B	2.01	13.75	2.34	2.07	0.12	0.20	2.01
		CC	S	0.91	0.17	0.77	0.16	0.86	0.84	0.91
			B	0.69	0.32	0.78	0.05	0.59	0.65	0.69
		RE (%)	S	16.39	67.20	3.35	67.73	6.55	18.39	16.39
			B	5.07	75.08	12.66	66.21	34.22	54.19	5.07
	CB4.2C	RMSE	S	2.19	9.27	1.61	2.02	0.15	0.17	2.19
			B	1.92	9.47	2.01	1.55	0.12	0.17	1.92
		CC	S	0.94	0.08	0.84	0.11	0.85	0.83	0.94
			B	0.66	0.44	0.85	0.01	0.53	0.68	0.66
		RE (%)	S	14.87	96.34	5.01	72.51	3.31	15.77	14.87
			B	2.84	70.18	8.77	57.09	34.88	55.36	2.84
	CB4.3C	RMSE	S	2.22	9.24	1.68	1.96	0.15	0.17	2.22
			B	1.95	8.35	1.89	1.45	0.12	0.17	1.95
		CC	S	0.95	0.11	0.87	−0.17	0.86	0.83	0.95
			B	0.66	0.39	0.87	−0.07	0.51	0.72	0.66
		RE (%)	S	15.01	111.78	7.59	66.46	1.29	5.14	15.01
			B	2.39	65.96	5.33	53.97	39.03	55.24	2.39
	CB5.1	RMSE	S	1.84	7.58	1.41	1.82	0.12	0.13	1.84
			B	1.97	7.48	2.02	1.16	0.11	0.16	1.97
		CC	S	0.95	0.27	0.89	−0.21	0.86	0.86	0.95
			B	0.64	0.48	0.85	0.09	0.52	0.74	0.64
		RE (%)	S	11.01	78.94	3.45	60.62	1.13	12.43	11.01
			B	0.52	63.00	6.76	36.34	43.19	65.12	0.52
Mid-lower bay	CB5.2	RMSE	S	1.69	6.23	1.20	1.67	0.13	0.13	1.69
			B	1.86	8.69	1.69	1.05	0.10	0.14	1.86
		CC	S	0.95	0.29	0.91	−0.26	0.84	0.84	0.95
			B	0.68	0.41	0.89	0.11	0.51	0.74	0.68
		RE (%)	S	9.36	66.84	4.90	51.28	3.52	14.03	9.36
			B	1.46	63.64	3.70	29.82	60.94	61.07	1.46
	CB5.4	RMSE	S	1.71	7.85	1.50	1.06	0.14	0.14	1.71
			B	2.24	7.20	1.77	1.02	0.09	0.11	2.24
		CC	S	0.94	0.23	0.85	−0.15	0.74	0.76	0.94
			B	0.68	0.39	0.89	−0.02	0.48	0.75	0.68
		RE (%)	S	8.20	71.59	9.36	7.44	10.64	20.02	8.20
			B	5.03	54.07	17.76	15.40	61.79	48.40	5.03
	CB6.1	RMSE	S	1.54	12.45	1.28	1.15	0.10	0.11	1.54
			B	2.30	12.30	2.05	1.03	0.06	0.08	2.30
		CC	S	0.90	0.12	0.84	−0.19	0.80	0.79	0.90
			B	0.76	0.09	0.93	0.11	0.72	0.78	0.76
		RE (%)	S	2.79	16.09	5.61	0.85	13.95	38.07	2.79
			B	5.93	38.12	28.52	15.94	27.26	42.34	5.93
	CB7.3	RMSE	S	2.32	4.99	1.27	1.14	0.06	0.06	2.32
			B	1.51	5.03	1.73	0.84	0.02	0.03	1.51
		CC	S	0.83	0.04	0.80	−0.04	0.77	0.74	0.83
			B	0.57	−0.06	0.81	−0.17	0.44	0.41	0.57
		RE (%)	S	2.72	36.79	6.89	12.31	10.83	53.86	2.72
			B	1.10	8.02	14.63	5.05	42.56	57.15	1.10
	WT5.1	RMSE	S	4.87	29.40	3.13	3.40	0.81	1.04	4.87
			B	9.57	13.80	4.44	3.92	0.85	0.85	9.57
		CC	S	0.74	0.29	0.47	−0.05	0.67	0.68	0.74
			B	0.59	0.17	0.85	−0.22	0.38	0.25	0.59

(continued)

TABLE 2. (continued)

Region	Station	Index	Layer	SAL	CHL	DO	NO_3^-	DIN	TON	TP
		RE (%)	S	53.34	44.13	11.90	94.04	130.97	166.46	53.34
			B	66.71	224.36	116.08	136.41	270.30	101.04	66.71
	LE2.3	RMSE	S	2.06	8.27	1.26	1.39	0.16	0.18	2.06
			B	2.79	7.31	1.67	1.48	0.14	0.16	2.79
		CC	S	0.92	0.17	0.89	−0.04	0.80	0.80	0.92
			B	0.75	0.33	0.95	−0.16	0.67	0.77	0.75
		RE (%)	S	11.53	49.04	7.11	36.49	17.56	40.77	11.53
			B	11.97	16.01	19.21	44.34	48.96	57.30	11.97
	LE3.4	RMSE	S	2.43	9.22	1.36	0.91	0.08	0.10	2.43
			B	3.25	NaN	1.88	1.25	0.09	0.12	3.25
		CC	S	0.93	−0.03	0.86	−0.01	0.45	0.40	0.93
			B	0.83	NaN	0.89	−0.35	0.53	1.00	0.83
		RE (%)	S	13.16	36.51	6.45	16.79	25.82	19.25	13.16
			B	16.84	NaN	10.40	23.77	24.89	793.57	16.84

CHL, chlorophyll a; DIN, dissolved inorganic nitrogen; NaN, no value; SAL, salinity; TON, total organic nitrogen; TP, total phosphorus.

In this test, the whole domain is smoothed with a volume-conservative filter (Ye et al. 2018), and the parameter settings are identical for both smoothed and non-smoothed cases. After bathymetry smoothing, the deepest part of the channel is up to 20 m shallower than that in the non-smoothed case, and correspondingly the shoals are deepened up to 13 m in the Eastern Shore of upper mid-Bay, thus effectively reducing the steep channel slopes (Figure 9a–9c). In most major tributaries such as the York River and the James River, the difference of the channel depths is up to 5 m, while for the Potomac River, the change is up to 12 m (Figure 9a–9c). To clearly show the effects on the vertical structures of state variables, we select one along-channel and three cross-channel transects. The along-channel transect follows the deepest region of its original bathymetry. Three typical cross-channel transects are chosen through the locations of the stations CB3.2, CB5.2, and CB6.4, which are near the Baltimore Harbor, the Potomac River, and the York River, respectively (Figure 9d). The alteration to the bathymetry is clearly seen in these transects: the smoothed case loses much of the deep channel but has deeper shoal areas (Figure 9e–9g).

One gross error from the bathymetry smoothing, which is often glossed over, is clearly seen in the profile comparisons such as Figure 9i: the observed and modeled profiles do not properly align vertically. Obviously, manipulations to force the two depths to be consistent with each other would lead to other artifacts. As shown in both along-channel and cross-channel profiles, there is less salt intrusion over the upper Bay in the main channel with the smoothed bathymetry (Figure 9h, 9i). For example, the bottom salinity around 39°N is about five PSU less than the observed bottom salinity (Figure 9i). The two cases result in quite different vertical profiles over the upper Bay channel, with the pycnocline being pushed too high relevant toward the water surface in the smoothed case, mostly due to shallower depth therein (Figure 9h, 9i). In the lower Bay, however, smoothing leads to a larger salt intrusion (Figures 9 and 10). The deepened depths in the shoal areas bring in saltier water there, and the reduced slopes increase the lateral exchange of salts and reduces lateral salinity gradients (Figure 9e–9g), which is a form of spurious diapycnal mixing (Zhang et al. 2016). The non-smoothed case has much deeper, narrower channels with steeper slopes, which leads to different lateral circulation patterns and sharper shoal-channel contrast (Ye et al. 2018) (Figure 10). In addition, the non-smoothed case has an overall stronger stratification, with a different mixing pattern from the smoothed case (Figure 13a–13c). Over the cross-channel transect closed to CB5.2, the non-smoothed case also has increased mixing near the deep slope (Figure 13b). We should remark that depending on the types of bathymetry smoothers used, the trend can be different from what is described here; however, in all cases, there are strong biases in the simulated salinity and lateral circulation patterns, and the shoal-channel contrast is always weakened. This has important implications for ecosystem functions as shown below.

Effects of Smoothed Bathymetry on Summer Hypoxia. Compare with observations, the non-smoothed case has a much better skill in capturing the hypoxia in the upper Bay (e.g., CB3.2) and major tributaries (e.g., the Potomac), partly because it simulates more accurate stratification and salt intrusion (Figure 11). Insufficient salt intrusion in these areas forbids the capture of hypoxia in the case of smoothed

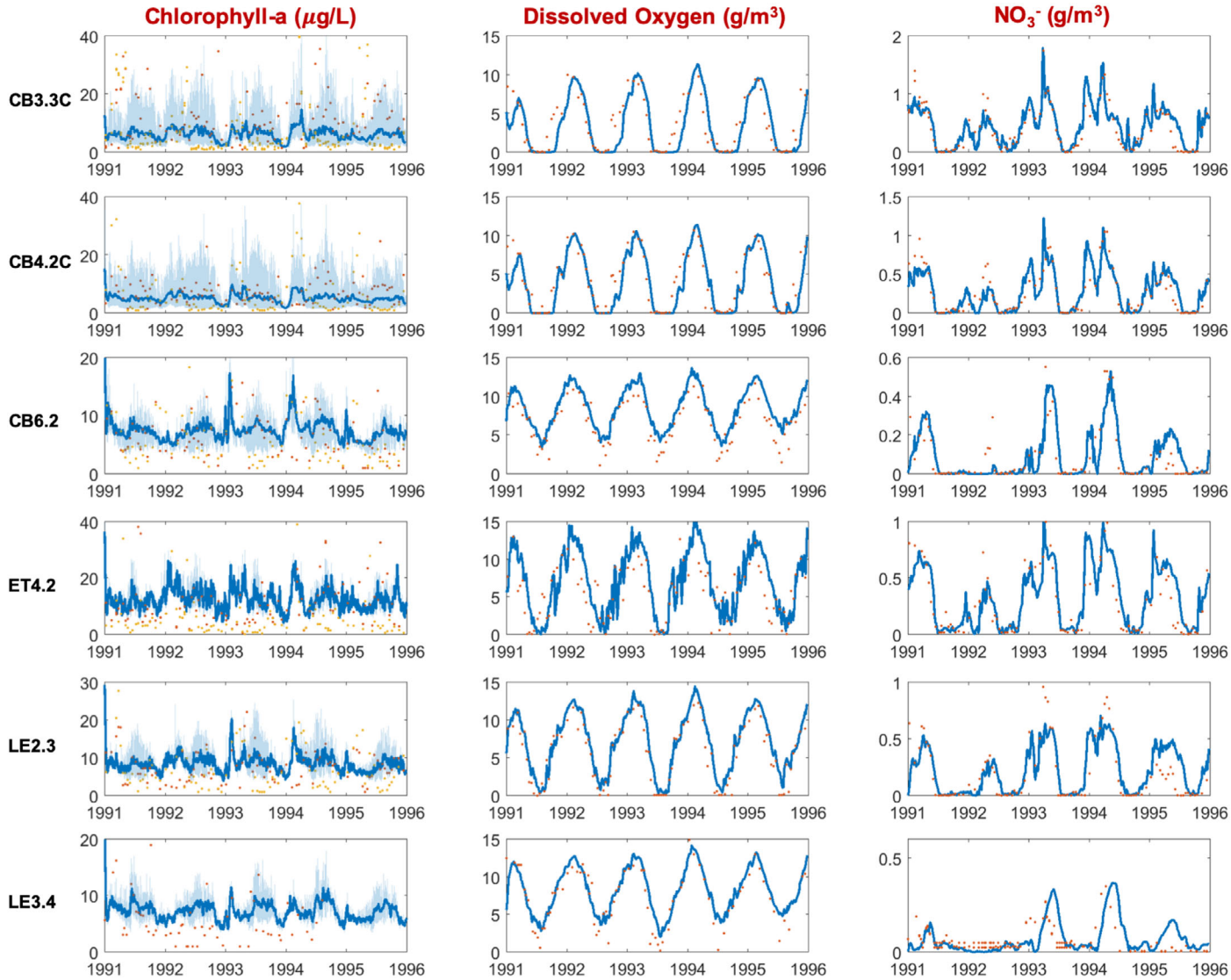

FIGURE 5. Time series of observed and modeled depth-averaged chlorophyll-a, bottom DO and surface nitrate at main stem station CB3.3C (upper-mid bay), CB4.2C (mid bay), CB6.2 (lower bay), and tributary stations ET4.2 (Chester R.), LE2.3 (Potomac R.) and LE3.4 (Rappahannock R.). In the chlorophyll-a plots, red spots represent surface observation, yellow ones represent bottom. Blue lines represent modeled concentrations, where dark ones represent depth-averaged values and light blue ones represent both surface and bottom concentrations. For other plots, red spots represent observed and blue lines represent modeled DO and nitrate.

bathymetry (more details of hypoxia in tributaries are discussed in Estimation of the Effects of Sea-Level Rise with Non-smoothed Bathymetry section). An important bias due to smoothing is found in the form of under-estimation of DO in the shoals of mid- and upper Bay so that it has an unrealistically broad hypoxia area (Figure 11), which is consistent with a broad and uniform salt intrusion pattern (cf. Figure 15; Ye et al. 2018). In the mid-Bay area, the larger lateral circulation brings the low-DO water in the channel to the shoals, resulting in mostly lower DO there if the bathymetry is smoothed (Figure 11). Due to the higher DO in the channel and lower DO in the shoal in the smoothed case than in the non-smoothed case, the total hypoxia volume, however, tends to be underestimated (cf. Figure 18).

Effects of Smoothed Bathymetry on Phytoplankton Production and Nutrient Budgets. Smoothing the bathymetry increases the shallow area (depth < 10 m) by about 230.5 km^2 (2.42%), which brings in more light supply for the whole Bay than the non-smoothed case to support phytoplankton production. The smoothing also decreases the depth of the mixing layer by about 1–2 m that tends to keep the phytoplankton stay near the surface (Figure 17c, 17d). As a result, in the smoothed case, the phytoplankton production

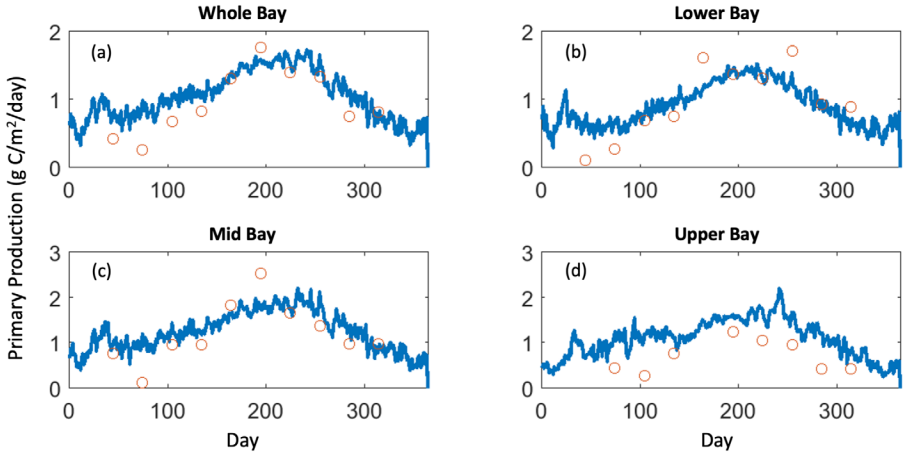

FIGURE 6. Comparison of daily results from the 5-year averaged modeled phytoplankton production with 17-year averaged observations (Harding et al. 2002) for (a) whole Bay, (b) lower Bay, (c) mid Bay, and (d) upper Bay. Blue lines represent model results and red circles represent observations.

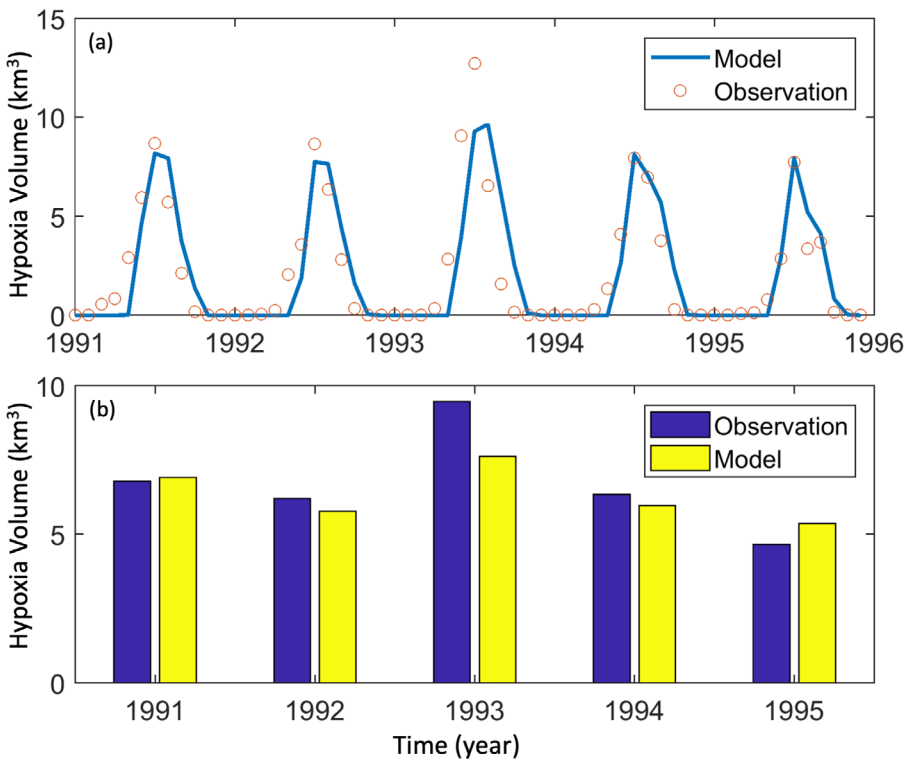

FIGURE 7. Comparison of (a) interpolated monthly averaged hypoxic volume from 1991 to 1995; (b) averaged hypoxic volume from June to August during each year of 1991–1995.

increases to more than 0.7 g C/m^2/day (Figure 12). In addition, the maximum phytoplankton production occurs in the channel slope between channel and shoal in non-smoothed case. This is because the areal phytoplankton production is limited by local volume and residence time (Qin and Shen 2017), and a sufficient large water depth is required to reach a high value. Another reason is that the shallow area often has a water depth less than the depth of euphotic zone, which limits phytoplankton to fully explore the light resource and hence limits the phytoplankton production (Cai et al. this issue). In the smoothed case, this region encroaches parts of the channel due to reduced slope.

Change of phytoplankton production can affect the annual budget of nutrients. To take total dissolved

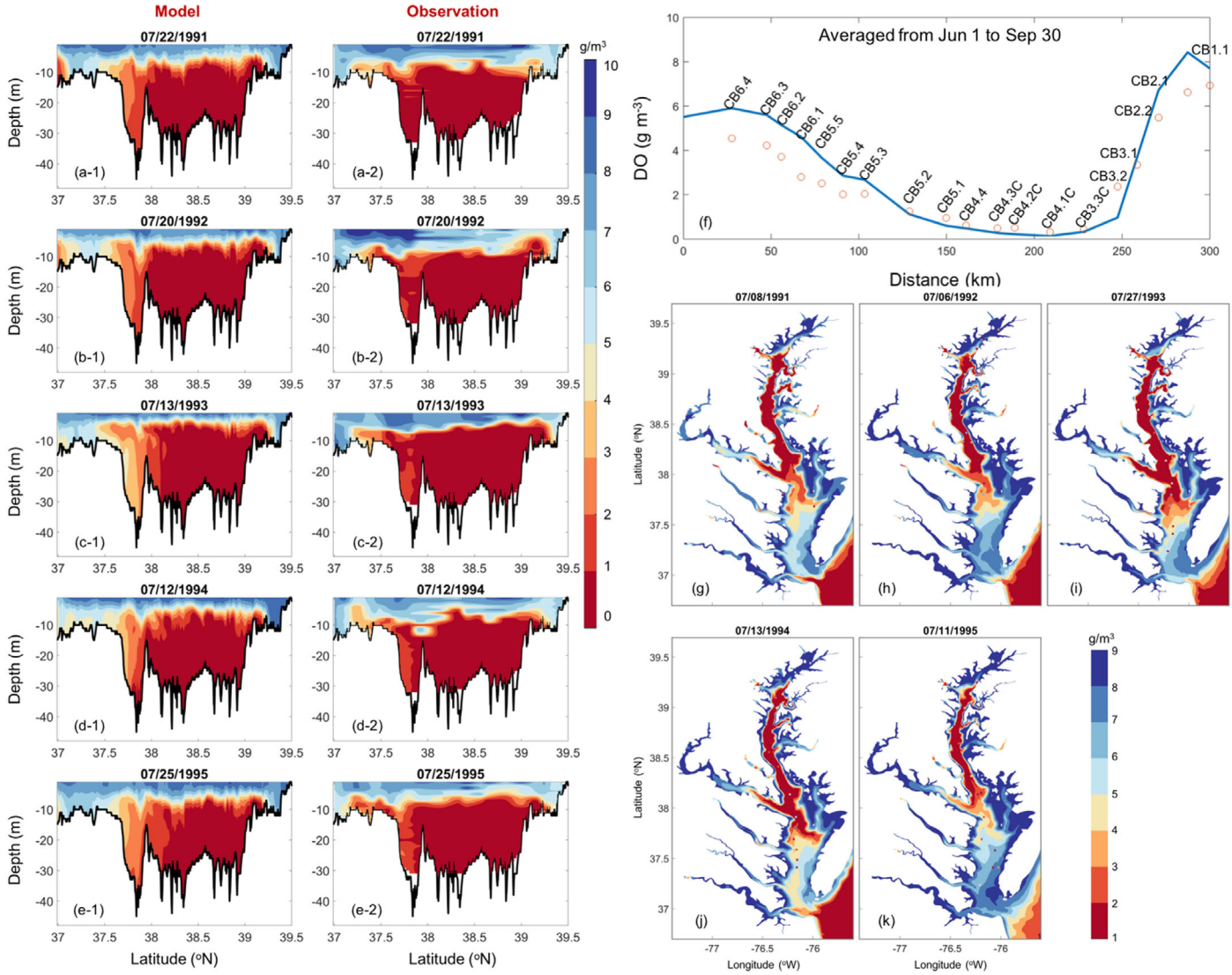

FIGURE 8. Snapshot comparison of modeled and observed DO vertical profile along main channel on (a-1,2) July 22, 1991, (b-1,2) July 20, 1992, (c-1,2) July 13, 1993, (d-1,2) July 12, 1994, and (e-1,2) July 25, 1995 over a 5-day window time. (f) Five-year averaged bottom DO from June to September along main channel stations. Blue line represents model results and red circles represent CBP observations. Comparison of modeled and observed bottom DO on (g) July 8, 1991, (h) July 6, 1992, (i) July 27, 1993, (j) July 13, 1994, and (k) July 11, 1995 over a 4-day window. The colored contours represent model results; the circles with gray "+" represent CBP observations on that day.

inorganic nitrogen as an example, the large depth-averaged concentration of channels in upper Bay spreads out to the shoal areas. Since most of the increase in phytoplankton production happens in upper Bay in the smoothed case, more DIN is consumed in this region. In the smoothed case, there is a decrease of about 0.1 g N/m^3 for depth-averaged DIN concentration in lower Bay. In terms of the whole water column, the decrease is about 1–3 g N/m^2.

Although the change in total production or total DIN budget is minor, bathymetry smoothing can make a difference up to more than 150% on production and 100% on DIN concentration in some shallow areas, which alternates the local distribution and events.

Freshwater age is another key indicator for assessing the impact of hydrodynamics and physical transport on the local biological processes. Compared to the non-smoothed case, the age of freshwater from Susquehanna River increases up to 40 days over the main Bay in the smoothed case (Figure 13c). Typically in the James River, which located closer to the bay mouth, an easier intrusion of aged water increases the water age toward the river head. While in the Rappahannock River, Choptank River, and Eastern Shore, where freshwater inflow is relatively small, smoothing induces more mixing which largely decreases the age of water in this region. Overall for the whole Bay, in the smoothed case the annually

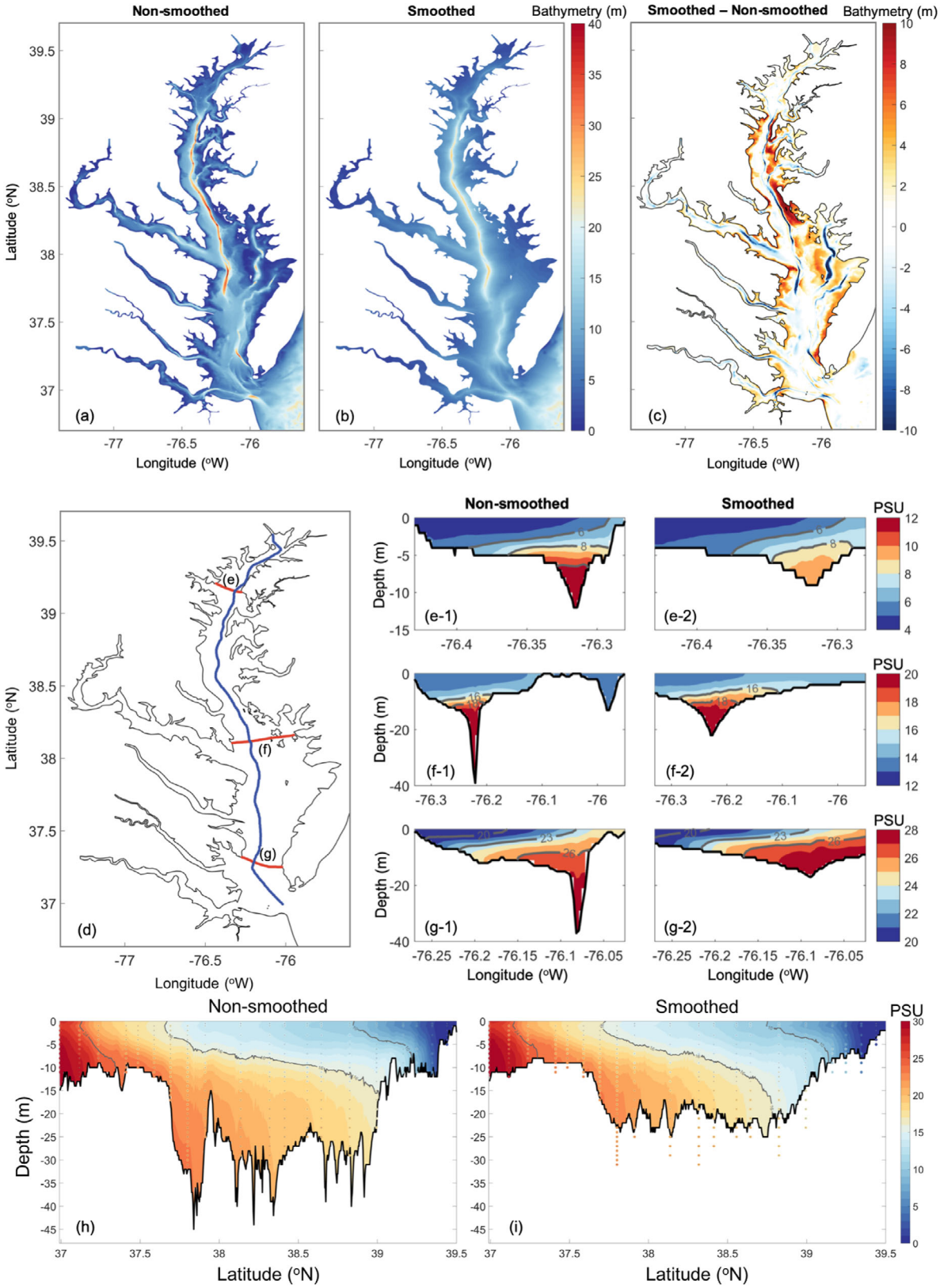

FIGURE 9. (a–c) Non-smoothed and smoothed bathymetry and their difference. (d). Locations of three cross-channel transects for (e–g) and one along-channel transect for (h,i), respectively. (e,f,g-1,2): Five-year averages of salinity over cross-channel transects located closed to CB3.2, CB5.2 and CB6.4 for the case of non-smoothed and smoothed bathymetry. (h,i): comparison for the along-channel transects; the colored contours represent model results; the circles with gray "+" represent CBP observations. Due to bathymetry alteration, the observed profiles are partially outside the model bottom in (i).

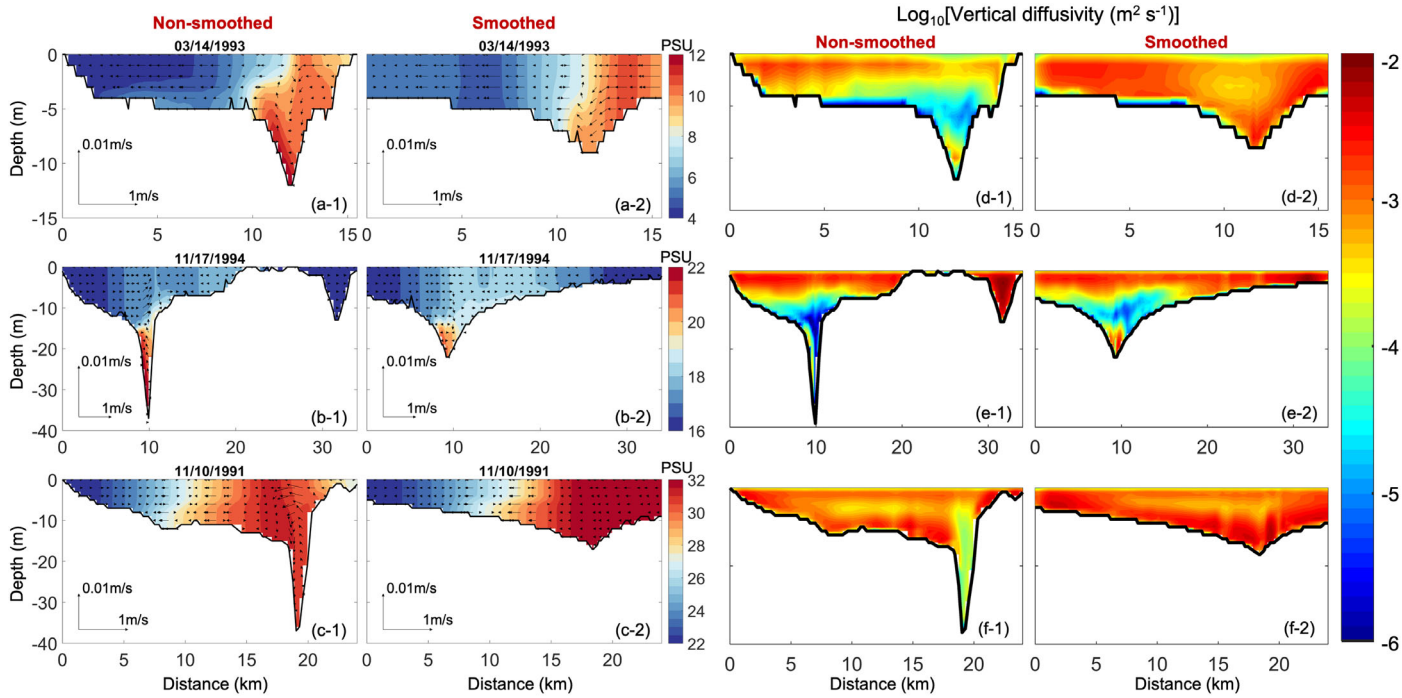

FIGURE 10. Screenshots of lateral circulation over cross-channel transects located closed to (a) CB3.2, (b) CB5.2, and (c) CB6.4 (transect shown in Figure 9) for the case of non-smoothed and smoothed bathymetry. The colored contours represent modeled salinity. The black arrows represent the flow direction along this transect with length proportional to the velocity magnitude. (d–f) Five-year-averages of vertical diffusivity in colored contours over cross-channel transects corresponded to (a–c) for the case of non-smoothed and smoothed bathymetry.

averaged age at Bay mouth increases 9–40 days (Figure 13e). This indicates a decrease in gravitational circulation in the smoothed case. The calculated total nitrogen export ratio (25%–40%) for without smoothing case is within a reasonable range from literature (Nixon et al. 1996). Wet year has smaller freshwater age along with larger nutrient export. The smoothed grid makes a difference of 2%–14% on total nitrogen export ratio, with large effects from wet or dry years (Figure 13d).

Grid Refinement in a Tributary

Baltimore Harbor is chosen for refinement because of its narrow channel and known severe hypoxia during summertime. While the narrow channel is often "widened" under bathymetry smoothing, we refined the grid to capture this key feature in the system. A finer grid is generated for the shipping channels to better capture the saltwater intrusion: the horizontal resolution is refined to ~300 × ~100 m in the along- and cross-channel directions, compared to ~500 × ~250 m in the original grid (Figure 14). The implicit scheme used in SCHISM ensures no penalty on the time steps (i.e., same time step is used for both grids).

Stronger salt intrusion to Baltimore Harbor is obtained with grid refinement. The known hypoxia in Baltimore Harbor is not simulated for the case of original grid and smoothed case, though the original non-smoothed one already simulated a more clear channel shape low-DO region than the smoothed case. The refined version has a more clear shape of hypoxia over this region (Figure 15). The seasonal variations of the refined case in Figure 16, compared with the original case, show significant improvement. The original grid was not able to simulate the stratification inside the harbor well so that there is little difference between the surface and the bottom chlorophyll-a in the original case. It has an over-estimated depth-averaged value and is not able to capture much of the observed surface algal blooms. In addition, the lack of strong stratification in the original grid also provides a significant amount of reaeration for bottom DO. The simulation of surface NO_3^- is also larger than observation but still has sensible inter-annual variations in the case of the original grid. Refinement of tributary resolution improves the simulation of physical transport, stratification, and therefore the relevant water quality variables. This sensitivity test tells the next step to refine the unstructured grid into small tributaries with non-smoothed bathymetry is a sensible direction with

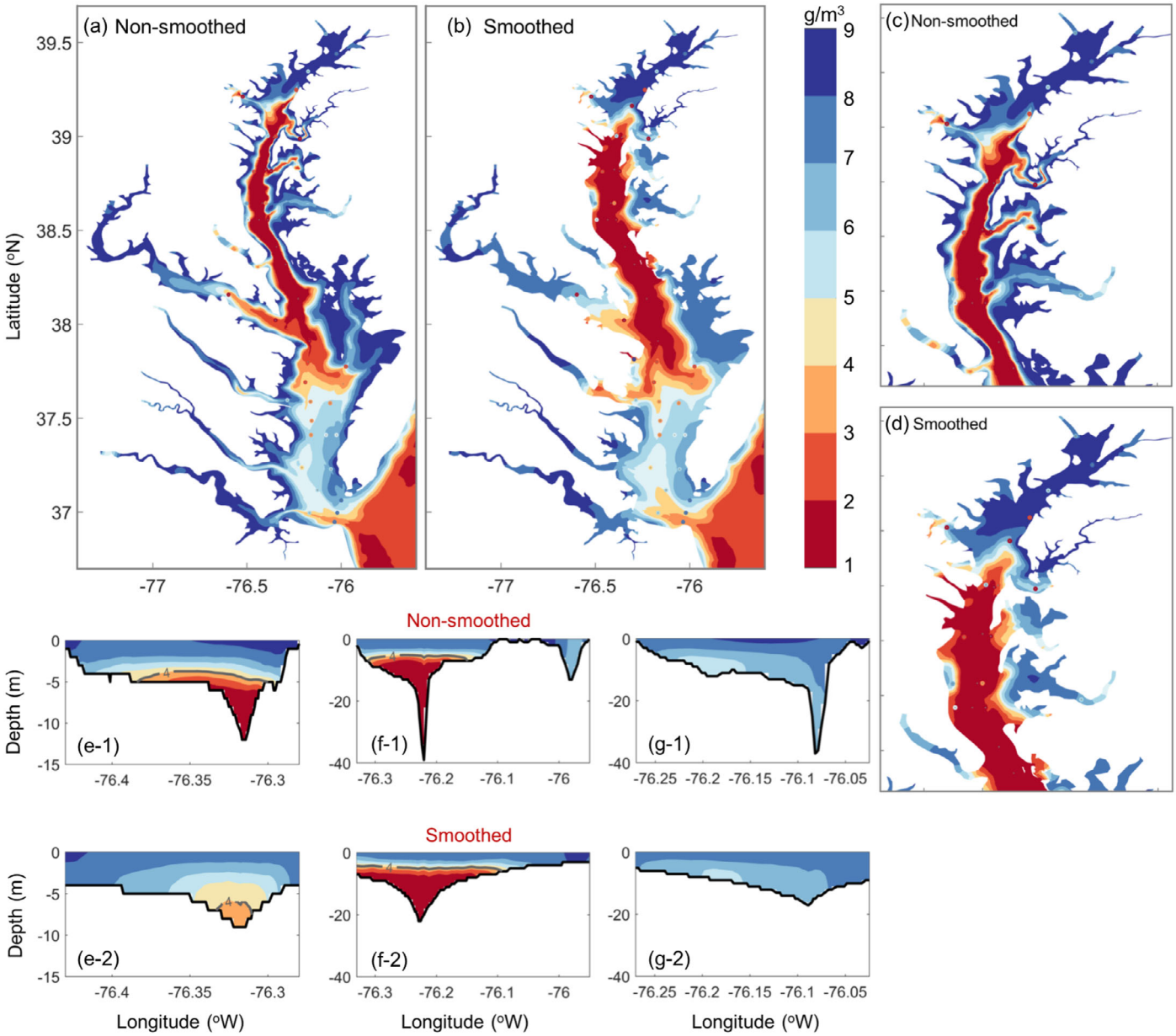

FIGURE 11. (a,b) Averaged bottom oxygen concentration on July 11, 1994 over a 4-day window for the case of non-smoothed and smoothed bathymetry. (c,d) Zoomed in to the Bay mouth for (a,b). The colored circles with grey "+" represent CBP observations in (a–d). (e,f,g-1,2): Five-year averages of oxygen concentration in July over cross-channel transects located closed to CB3.2, CB5.2, and CB6.4 (transects shown in Figure 9) for the cases of non-smoothed and smoothed bathymetry, respectively.

relatively low cost of computational efficiency (5% increased computational time in the refined case due to the increased grid size).

Estimation of the Effects of Sea-Level Rise with Non-Smoothed Bathymetry

We will briefly discuss the impact of bathymetry smoothing on the prediction of the trend under Sea-Level Rise (SLR) for salinity and DO here and leave the more detailed discussion to the sequel paper (Cai et al. this issue). The SLR effects consist of both physical effects on the estuarine circulation, salt intrusion, and flooding, and indirect effects on hypoxia and biogeochemical processes.

Two SLR (+0.5 m) cases are conducted based on the two cases (non-smoothed and smoothed) discussed in Importance of Bathymetry on Simulating Hypoxia in Chesapeake Bay section. The increase of 0.5 m is applied at the ocean boundary while the rest of the model setup is kept the same.

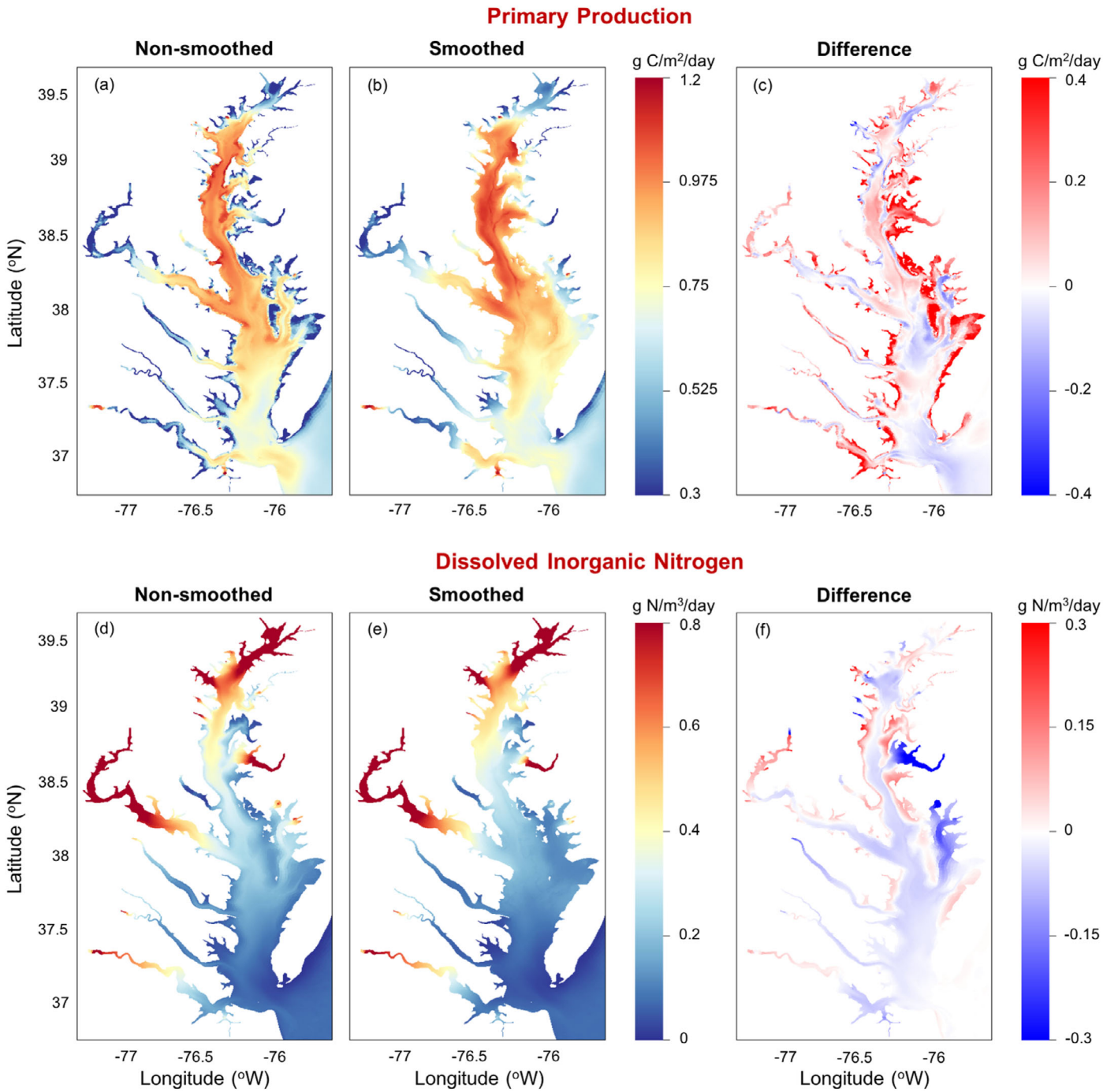

FIGURE 12. (a,b) Five-year averages of phytoplankton production for the case of non-smoothed and smoothed bathymetry; (c) difference of phytoplankton production; (d,e) DIN concentration for the case of non-smoothed and smoothed bathymetry; (f) difference of DIN concentration (difference = smoothed minus non-smoothed).

Overall, the smoothed case predicts larger salt intrusion caused by SLR (Figure 17a, 17b). In the non-smoothed case, the average increase is 0.79 PSU over the transect along the main channel and 0.81 PSU for the bottom salinity of the Bay; these are increased by 22.8% and 13.6%, respectively, under the smoothed case. The predicted increase in salt intrusion is more uniform both vertically and horizontally over the main stem in the case of smoothed bathymetry, while in the case of non-smoothed bathymetry, the increase in salinity is mostly concentrated in the upper 10 m of the water column (thus moving the halocline upward), and a less increase occurs in the deep channels (Figure 17a, 17b). Along the main

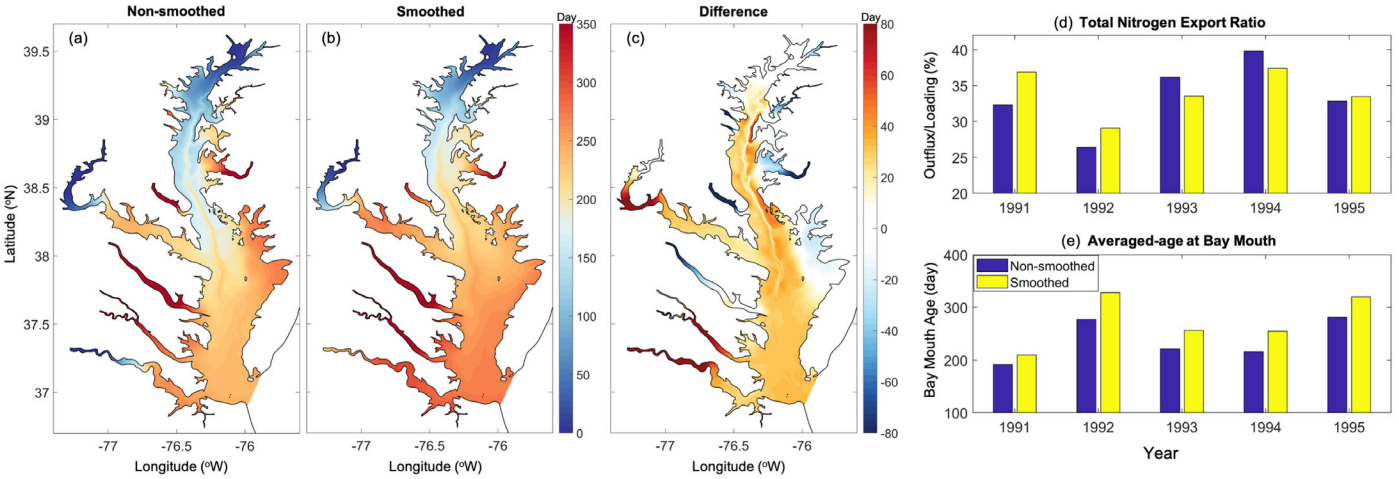

FIGURE 13. (a,b) Five-year averages of freshwater age from Susquehanna River (depth-averaged) for the case of non-smoothed and smoothed bathymetry. (c) Five-year averaged difference of depth-averaged freshwater age between these two cases (smoothed minus non-smoothed). (d) Total nitrogen export ratio (outflux divided by loading) of each year. (e) Bay-mouth depth-averaged water age of each year for the case of non-smoothed and smoothed bathymetry. Blue bar represents non-smoothed case and yellow bar represents smoothed case.

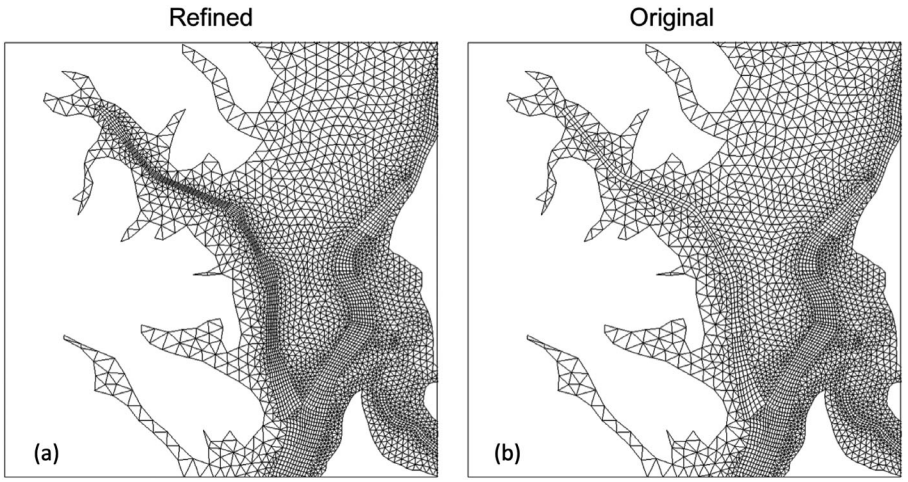

FIGURE 14. Unstructured (a) refined and (b) original mesh from main channel into Baltimore Harbor.

channel, the largest increase in salinity occurs near 39.25°N (CB3.2; Figure 17a). More exaggerated changes occur in some tributaries for the case of smoothed bathymetry, and the salinity even decreases in some western tributaries (Figure 17b). These changes are highly questionable, which demonstrates the significance of using the unsmoothed representation of bathymetry with the UG grid in the SLR study (Cai et al. this issue).

The total hypoxia volume tends to be underestimated in the smoothed case by up to 3 km^3 (~2 km^3 for the July period) (Figure 18a). More importantly, the change in the hypoxic volume due to SLR is exaggerated by ~2.5 km^3 (or 100% off) for the July period (Figure 18b). This is consistent with the exaggerated change in salt intrusion in the entire system (Figure 17).

Model Uncertainties and Limitations

We briefly discuss the remaining model uncertainties. Due to the scarcity of observations outside the Bay, there are uncertainties associated with the open boundary conditions, although we have partially mitigated this by extending the domain to the shelf break. To assess the uncertainties, we compare results from the base with some extreme/unrealistic tests. In the first test, algae are not allowed to grow outside the Bay, since we usually assign the same

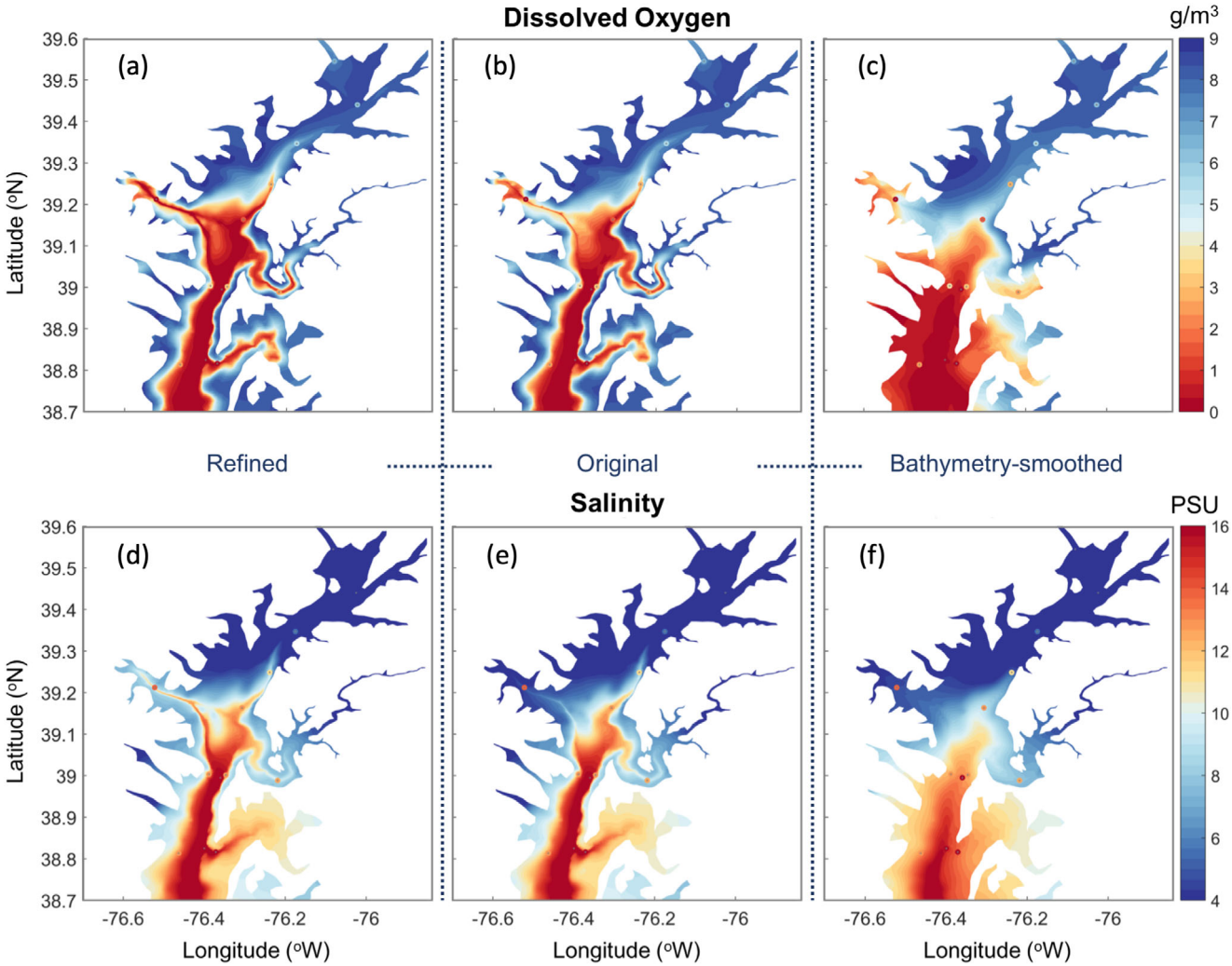

FIGURE 15. Five-year averages of bottom oxygen concentration and salinity over Baltimore Harbor in July for the case of (a,d) refined grid (without bathymetry smoothing), original grid with (b,e) non-smoothed and (c,f) smoothed bathymetry, respectively. The colored contours represent model results; the circles with gray "+" represent CBP observations.

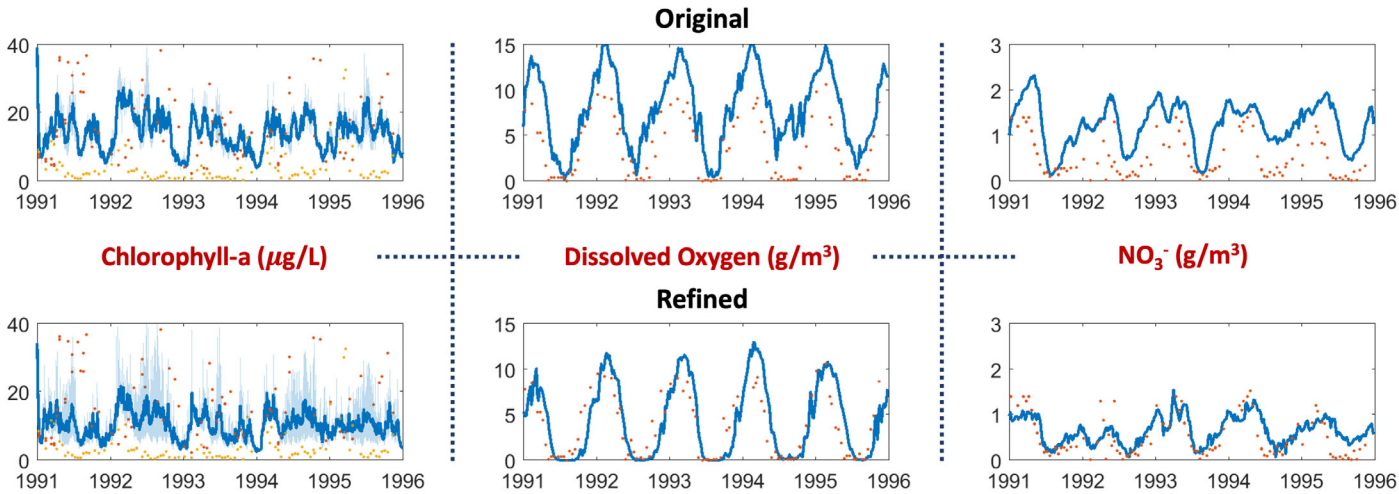

FIGURE 16. Comparison of depth-averaged (dark blue line), bottom and surface (light blue lines) chlorophyll-a, bottom DO, and surface nitrite at WT5.1 (cf. Figure 3). Dots represent CBP observations. Red dots in plots of chlorophyll-a represent surface and yellow ones represent bottom.

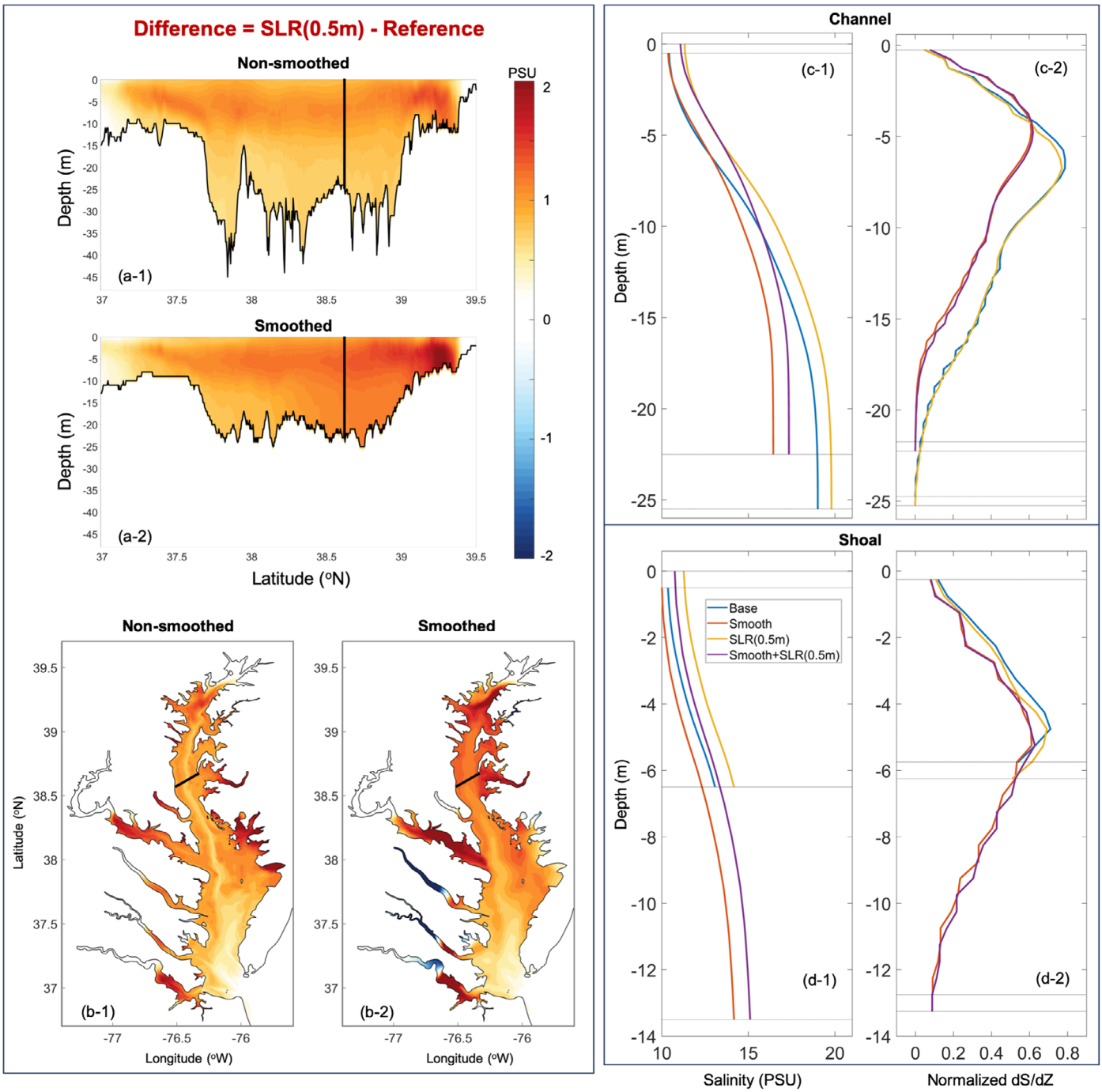

FIGURE 17. Five-year averages of (a) along-channel salinity difference and (b) bottom salinity difference caused by Sea-Level Rise (SLR) for non-smoothed and smoothed cases. Salinity profile and normalized ds/dz for (c) channel and (d) shoal marked black in (a,b).

groups and parameters for the algae in/outside the Bay. In the second and third tests, we increase the averaged TIP concertation from 0.035 to 0.06 g/m^3 and decrease it to 0.01 g/m^3, respectively, at the boundary. The two tests are used to investigate the impact of the net influx of phosphorus from the Bay mouth on the DO dynamics in the Bay, since it has been suggested that the coast input of phosphorus has a significant effect on the phytoplankton production in estuarine systems (Nixon et al. 1996).

Our results show little effect from the changes in the boundary conditions on the simulated summer hypoxia over the upper Bay, with an overall difference of <0.6 g/m^3 in winter (Figure 19). The middle Bay and lower Bay receive a greater influence, but the difference is basically smaller than 1 g/m^3. If

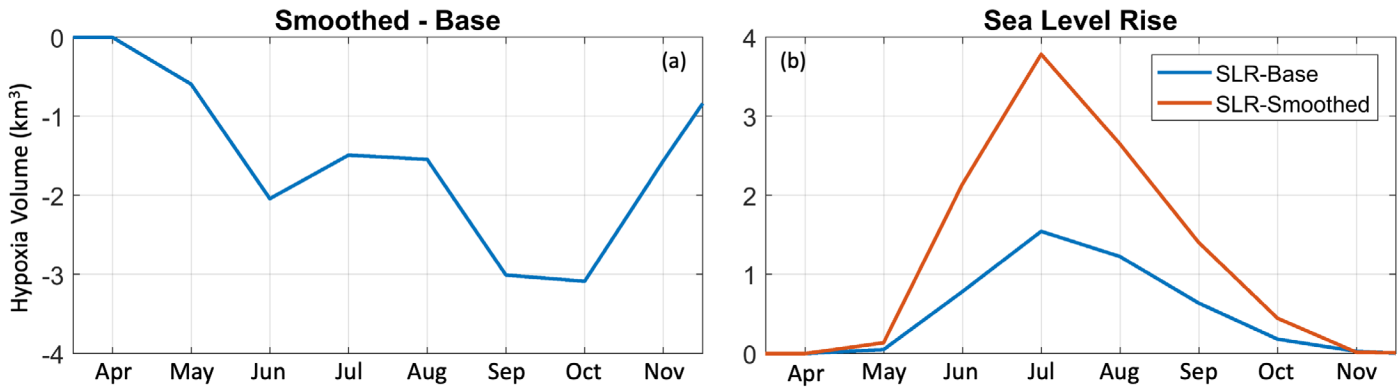

FIGURE 18. (a) Difference of simulated hypoxic volume as the result of bathymetry smoothing. (b) Change of hypoxia volume caused by SLR (0.5 m) for non-smoothed and smoothed cases.

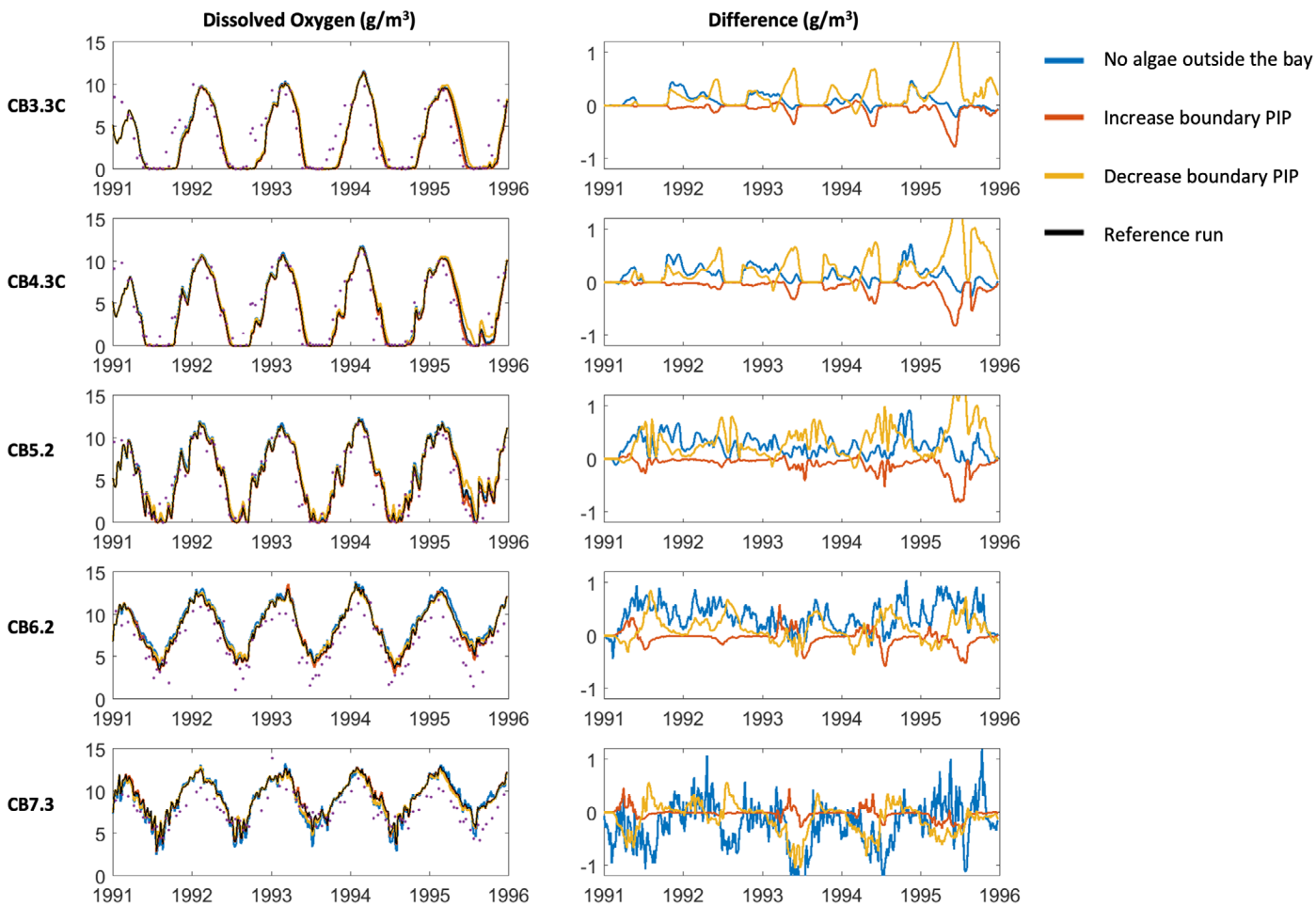

FIGURE 19. Time series of DO concertation and the difference to the reference run (test — reference) in typical stations along the main stem over different regions. Purple dots represent CBP observations.

there is no algal growth outside the Bay, there will be less oxygen consumption inside the Bay except for the region closed to the mouth. Increasing or decreasing outside particulate inorganic phosphorus slightly decreases or increases bottom DO concertation in most regions except for the area closed to the Bay mouth. Decreasing boundary inorganic phosphorus causes a larger change on bottom oxygen concertation than increasing it in most of the Bay areas, which indicates that phosphorus is limited inside the

hypoxia zone. Overall, the influence of boundary conditions at the shelf break seems minor.

In this study, the three groups of phytoplankton are the only primary producers in the model. Besides phytoplankton, other primary producers, such as benthic algae, marsh, SAV (submerged aquatic vegetation), and macroalgae could play a significant role over shallow areas under certain conditions (Qin and Shen 2019). The potential contributions of other producers, especially for shallow areas are not included since the focus here is the main stem. An SAV model has already been developed inside the framework of SCHISM-ICM (Cai 2018; Zhang et al. 2020) and others may be added in the future.

SUMMARY AND CONCLUSION

We have successfully applied the SCHISM-ICM to the simulation of water quality with a focus of hypoxia in Chesapeake Bay. The model shows a good performance in simulating dynamics of water quality variables such as chlorophyll-a, DO, nutrients, and phytoplankton productions. The bias of estimated hypoxic volume from model and observation is generally smaller than 1 km^3.

Sensitivity test results with bathymetry smoothing are found to be fundamentally inaccurate. Bathymetry smoothing alters the physical environment of the system, and hence has cascade implications on the simulations of the ecosystem, including over-estimation of bottom DO in the channel and tributaries and under-estimation over the shoal. The smoothing also increases depths of shallow-water areas, and leads to an increase in phytoplankton production up to 150% in some localized areas and a difference of 2%–14% in nutrient export, partly due to the increased freshwater age. Comparisons with observations clearly demonstrate that it is important to use realistic bathymetry (with aid from high resolution) to provide accurate simulations for physical and biogeochemical processes, and to correctly predict the impact of sea-level rise on future summertime hypoxia, which is of great concern for the Bay management. The seamless cross-scale capability of SCHISM-ICM, together with its efficiency and robustness, can be effectively utilized as a powerful tool for adaptive management.

ACKNOWLEDGMENTS

This work is partially supported by California Department of Water Resources and VIMS Graduate Research Grants. We have also received generous help from USEPA's CBP. This is Contribution No. 3956 of the Virginia Institute of Marine Science, William & Mary.

Simulations presented in this paper were conducted using the following computational facilities: (1) Sciclone at the College of William and Mary which were provided with assistance from the National Science Foundation, the Virginia Port Authority, Virginia's Commonwealth Technology Research Fund, and the Office of Naval Research; (2) the Extreme Science and Engineering Discovery Environment (XSEDE; Grant TG-OCE130032), which is supported by National Science Foundation, USA Grant Number OCI-1053575; (3) the NASA High-End Computing (HEC) Program through the NASA Advanced Supercomputing (NAS) Division at Ames Research Center; and (4) U.S. Department of Energy's Scientific Computing Center.

AUTHORS' CONTRIBUTIONS

Xun Cai: Conceptualization; data curation; formal analysis; investigation; methodology; resources; software; validation; visualization; writing-original draft; and writing-review and editing. **Yinglong J. Zhang:** Conceptualization; funding acquisition; investigation; methodology; project administration; resources; software; supervision; and writing-review and editing. **Jian Shen:** Conceptualization; data curation; methodology; supervision; validation; and writing-review and editing. **Harry Wang:** Methodology; software. **Zhengui Wang:** Methodology; software. **Qubin Qin:** Conceptualization; investigation; and writing-review and editing. **Fei Ye:** Resources; software.

LITERATURE CITED

Bever, A.J., M.A. Friedrichs, C.T. Friedrichs, M.E. Scully, and L.W. Lanerolle. 2013. "Combining Observations and Numerical Model Results to Improve Estimates of Hypoxic Volume Within the Chesapeake Bay, USA." *Journal of Geophysical Research: Oceans* 118 (10): 4924–44. https://doi.org/10.1002/jgrc.20331.

Brown, C.W., R.R. Hood, W. Long, J. Jacobs, D.L. Ramers, C. Wazniak, J.D. Wiggert, R. Wood, and J. Xu. 2013. "Ecological Forecasting in Chesapeake Bay: Using A Mechanistic-Empirical Modeling Approach." *Journal of Marine Systems* 125: 113–25. https://doi.org/10.1016/j.jmarsys.2012.12.007.

Cai, X.2018. "Impact of Submerged Aquatic Vegetation on Water Quality in Cache Slough Complex, Sacramento-San Joaquin Delta: A Numerical Modeling Study." Master thesis, College of William and Mary. https://doi.org/10.25773/v5-8snw-1660.

Cai, X., J. Shen, Y.J. Zhang, Q. Qin, Z. Wang, and H. Wang. this issue. "Impacts of Sea Level Rise on Hypoxia and Phytoplankton Production in Chesapeake Bay: Model Prediction and Assessment". *Journal of the American Water Resources Association*.

Cerco, C.F. 1995. "Simulation of Long-Term Trends in Chesapeake Bay Eutrophication." *Journal of Environmental Engineering* 121 (4): 298–310. https://doi.org/10.1061/(ASCE)0733-9372(1995)121:4(298).

Cerco, C.F. 2000. "Phytoplankton Kinetics in the Chesapeake Bay Eutrophication Model." *Water Quality and Ecosystems Modeling* 1 (1–4): 5–49. https://doi.org/10.1023/A:1013964231397.

Cerco, C.F., and T.M. Cole. 1994. *CE-QUAL-ICM: a Three-Dimensional Eutrophication Model, Version 1.0. User's Guide*. Vicksburgh, MS: U.S. Army Corps of Engineers Waterways Experiments Station.

Cerco, C.F., and M.R. Noel. 2013. "Twenty-One-Year Simulation of Chesapeake Bay Water Quality Using the CE-QUAL-ICM Eutrophication Model." *Journal of the American Water Resources Association* 49 (5): 1119–33. https://doi.org/10.1111/jawr.12107.

Deleersnijder, E., J.M. Campin, and E.J. Delhez. 2001. "The Concept of Age in Marine Modelling: I. Theory and Preliminary Model Results." *Journal of Marine Systems* 28 (3–4): 229–67. https://doi.org/10.1016/S0924-7963(01)00026-4.

Di Toro, D.M., and J.J. Fitzpatrick. 1993. "Chesapeake Bay Sediment Flux Model." Final Report (No. AD-A-267189/9/XAB). Mahwah, NJ: Hydroqual Inc.

Feng, Y., M.A. Friedrichs, J. Wilkin, H. Tian, Q. Yang, E.E. Hofmann, J.D. Wiggert, and R.R. Hood. 2015. "Chesapeake Bay Nitrogen Fluxes Derived from A Land-Estuarine Ocean Biogeochemical Modeling System: Model Description, Evaluation, and Nitrogen Budgets." *Journal of Geophysical Research: Biogeosciences* 120 (8): 1666–95. https://doi.org/10.1002/2015JG002931.

Harding, L.W. Jr, M.E. Mallonee, and E.S. Perry. 2002. "Toward a Predictive Understanding of Primary Productivity in a Temperate, Partially Stratified Estuary." *Estuarine, Coastal and Shelf Science* 55 (3): 437–63. https://doi.org/10.1006/ecss.2001.0917.

Irby, I.D., M.A. Friedrichs, C.T. Friedrichs, A. Bever, R.R. Hood, L.W. Lanerolle, M. Li et al. 2016. "Challenges Associated with Modeling Low-Oxygen Waters in Chesapeake Bay: A Multiple Model Comparison." *Biogeosciences* 13 (7): 2011. https://doi.org/10.5194/bgd-12-20361-2015.

Kemp, W.M., W.R. Boynton, J.E. Adolf, D.F. Boesch, W.C. Boicourt, G. Brush, J.C. Cornwell et al. 2005. "Eutrophication of Chesapeake Bay: Historical Trends and Ecological Interactions." *Marine Ecology Progress Series* 303: 1–29. https://doi.org/10.3354/meps303001.

Kemp, W.M., P.A. Sampou, J. Garber, J. Tuttle, and W.R. Boynton. 1992. "Seasonal Depletion of Oxygen from Bottom Waters of Chesapeake Bay: Roles of Benthic and Planktonic Respiration and Physical Exchange Processes." *Marine Ecology Progress Series* 85: 137–52. www.jstor.org/stable/24829928.

Lanerolle, L.W., R.C. Patchen, and F. Aikman. 2010. "The Second Generation Chesapeake Bay Operational Forecast System (CBOFS2): A ROMS-Based Modeling System." In *Estuarine and Coastal Modeling*, 621–42. https://doi.org/10.1061/41121(388)37.

Lee, Y.J., W.R. Boynton, M. Li, and Y. Li. 2013. "Role of Late Winter-Spring Wind Influencing Summer Hypoxia in Chesapeake Bay." *Estuaries and Coasts* 36 (4): 683–96. https://doi.org/10.1007/s12237-013-9592-5.

Li, M., L. Zhong, and L.W. Harding. 2009. "Sensitivity of Plankton Biomass and Productivity to Variations in Physical Forcing and Biological Parameters in Chesapeake Bay." *Journal of Marine Research* 67 (5): 667–700. https://doi.org/10.1357/002224009791218878.

Mesinger, F., G. DiMego, E. Kalnay, K. Mitchell, P.C. Shafran, W. Ebisuzaki, D. Jović et al. 2006. "North American Regional Reanalysis." *Bulletin of the American Meteorological Society* 87 (3): 343–60. https://doi.org/10.1175/BAMS-87-3-343.

Murphy, R.R., W.M. Kemp, and W.P. Ball. 2011. "Long-term Trends in Chesapeake Bay Seasonal Hypoxia, Stratification, and Nutrient Loading." *Estuaries and Coasts* 34 (6): 1293–309. https://doi.org/10.1007/s12237-011-9413-7.

Newcombe, C.L., and W.A. Horne. 1938. "Oxygen-poor Waters of the Chesapeake Bay." *Science* 88 (2273): 80–81. https://doi.org/10.1126/science.88.2273.80.

Nixon, S.W. 1995. "Coastal Marine Eutrophication: A Definition, Social Causes, and Future Concerns." *Ophelia* 41 (1): 199–219. https://doi.org/10.1080/00785236.1995.10422044.

Nixon, S.W., J.W. Ammerman, L.P. Atkinson, V.M. Berounsky, G. Billen, W.C. Boicourt, W.R. Boynton et al. 1996. "The Fate of Nitrogen and Phosphorus at the Land-Sea Margin of the North Atlantic Ocean." *Biogeochemistry* 35 (1): 141–80. https://doi.org/10.1007/BF02179826.

Park, K., A.Y. Kuo, J. Shen, and J.M. Hamrick. 1995. "A Three-Dimensional Hydrodynamic-Eutrophication Model (HEM-3D): Description of Water Quality and Sediment Process Submodels." Special report in applied marine science and ocean engineering, no. 327. Virginia Institute of Marine Science, College of William and Mary. https://doi.org/10.21220/V5ZH9N.

Qin, Q., and J. Shen. 2017. "The Contribution of Local and Transport Processes to Phytoplankton Biomass Variability over Different Timescales in the Upper James River, Virginia." *Estuarine, Coastal and Shelf Science* 196: 123–33. https://doi.org/10.1016/j.ecss.2017.06.037.

Qin, Q., and J. Shen. 2019. "Pelagic Contribution to Gross Primary Production Dynamics in Shallow Areas of York River, VA, USA." *Limnology and Oceanography* 64 (4): 1484–99. https://doi.org/10.1002/lno.11129.

Seliger, H.H., J.A. Boggs, and W.H. Biggley. 1985. "Catastrophic Anoxia in the Chesapeake Bay in 1984." *Science* 228 (4695): 70–73. https://doi.org/10.1126/science.228.4695.70.

Shen, J., and L. Haas. 2004. "Calculating Age and Residence Time in the Tidal York River Using Three-Dimensional Model Experiments." *Estuarine, Coastal and Shelf Science* 61 (3): 449–61. https://doi.org/10.1016/j.ecss.2004.06.010.

Shenk, G.W., and L.C. Linker. 2013. "Development and Application of the 2010 Chesapeake Bay Watershed Total Maximum Daily Load Model." *Journal of the American Water Resources Association* 49 (5): 1042–56. https://doi.org/10.1111/jawr.12109.

Taft, J.L., W.R. Taylor, E.O. Hartwig, and R. Loftus. 1980. "Seasonal Oxygen Depletion in Chesapeake Bay." *Estuaries* 3 (4): 242–47. http://www.jstor.com/stable/1352079.

Testa, J.M., Y. Li, Y.J. Lee, M. Li, D.C. Brady, D.M. Di Toro, W.M. Kemp, and J.J. Fitzpatrick. 2014. "Quantifying the Effects of Nutrient Loading on Dissolved O_2 Cycling and Hypoxia in Chesapeake Bay Using A Coupled Hydrodynamic-Biogeochemical Model." *Journal of Marine Systems* 139: 139–58. https://doi.org/10.1016/j.jmarsys.2014.05.018.

U.S. Environmental Protection Agency (USEPA). 2003. "*Ambient water quality criteria for dissolved oxygen, water clarity and chlorophyll a for the Chesapeake Bay and its tidal tributaries*." Annapolis, MD: Region III, Chesapeake Bay Program Off. Rep. EPA-903-R-03-002, 343 pp.

Xia, M., and L. Jiang. 2016. "Application of an Unstructured Grid-Based Water Quality Model to Chesapeake Bay and Its Adjacent Coastal Ocean." *Journal of Marine Science and Engineering* 4 (3): 52. https://doi.org/10.3390/jmse4030052.

Xu, J., and R.R. Hood. 2006. "Modeling Biogeochemical Cycles in Chesapeake Bay with a Coupled Physical-Biological Model." *Estuarine, Coastal and Shelf Science* 69 (1–2): 19–46. https://doi.org/10.1016/j.ecss.2006.03.021.

Ye, F., Y.J. Zhang, M.A. Friedrichs, H.V. Wang, I.D. Irby, J. Shen, and Z. Wang. 2016. "A 3D, Cross-Scale, Baroclinic Model with Implicit Vertical Transport for the Upper Chesapeake Bay and Its Tributaries." *Ocean Modelling* 107: 82–96. https://doi.org/10.1016/j.ocemod.2016.10.004.

Ye, F., Y.J. Zhang, H.V. Wang, M.A. Friedrichs, I.D. Irby, E. Alteljevich, A. Valle-Levinson et al. 2018. "A 3D Unstructured-Grid Model for Chesapeake Bay: Importance of Bathymetry." *Ocean Modelling* 127: 16–39. https://doi.org/10.1016/j.ocemod.2018.05.002.

Zhang, Y.J., E. Ateljevich, H.C. Yu, C.H. Wu, and C.S. Jason. 2015. "A New Vertical Coordinate System for a 3D Unstructured-Grid Model." *Ocean Modelling* 85: 16–31. https://doi.org/10.1016/j.ocemod.2014.10.003.

Zhang, Y., and A.M. Baptista. 2008. "SELFE: A Semi-Implicit Eulerian-Lagrangian Finite-Element Model for Cross-Scale Ocean Circulation." *Ocean modelling* 21 (3–4): 71–96. https://doi.org/10.1016/j.ocemod.2007.11.005.

Zhang, Y.J., N. Gerdts, E. Ateljevich, and K. Nam. 2020. "Simulating Vegetation Effects on Flows in 3D Using an Unstructured Grid Model: Model Development and Validation." *Ocean Dynamics* 70 (2): 213–30. https://doi.org/10.1007/s10236-019-01333-8.

Zhang, Y.J., F. Ye, E.V. Stanev, and S. Grashorn. 2016. "Seamless Cross-Scale Modeling with SCHISM." *Ocean Modelling* 102: 64–81. https://doi.org/10.1016/j.ocemod.2016.05.002.